THE JOURNAL OF BIOLOGICAL CHEMISTRY
Vol. 279, No. 30, Issue of July 23, pp. 31556–31567, 2004
Printed in U.S.A.

Redox-regulated Turnover of Nrf2 Is Determined by at Least Two Separate Protein Domains, the Redox-sensitive Neh2 Degron and the Redox-insensitive Neh6 Degron*[S]

Received for publication, March 19, 2004, and in revised form, May 12, 2004
Published, JBC Papers in Press, May 13, 2004, DOI 10.1074/jbc.M403061200

Michael McMahon‡§, Nerys Thomas‡, Ken Itoh¶, Masayuki Yamamoto¶, and John D. Hayes‡

From the ‡Biomedical Research Centre, Ninewells Hospital and Medical School, University of Dundee, Dundee DD1 9SY, Scotland, United Kingdom and ¶Centre for Tsukuba Advanced Research Alliance and Institute of Basic Medical Sciences, University of Tsukuba, Tsukuba 305-8577, Japan

The Nrf2 transcription factor is more rapidly turned over in cells grown under homeostatic conditions than in those experiencing oxidative stress. The variable turnover of Nrf2 is accomplished through the use of at least two degrons and its redox-sensitive interaction with the Kelch-repeat protein Keap1. In homeostatic COS1 cells, the Neh2 degron confers on Nrf2 a half-life of less than 10 min. Analyses of deletion mutants of a Gal4(HA)mNeh2 fusion protein and full-length mNrf2 indicate that full redox-sensitive Neh2 destabilizing activity depends upon two separate sequences within this N-terminal domain. The DIDLID element (amino acids 17–32) is indispensable for Neh2 activity and appears necessary to recruit a ubiquitin ligase to the fusion protein. A second motif within Neh2, the ETGE tetrapeptide (amino acids 79–82), allows the redox-sensitive recruitment of Nrf2 to Keap1. This interaction, which occurs only in homeostatic cells, enhances the capacity of the Neh2 degron to direct degradation by functioning downstream of ubiquitination mediated by the DIDLID element. By contrast with the situation under homeostatic conditions, the Neh2 degron is neither necessary nor sufficient to account for the characteristic half-life of Nrf2 in oxidatively stressed cells. Instead, the previously uncharacterized, redox-insensitive Neh6 degron (amino acids 329–379) is essential to ensure that the transcription factor is still appropriately turned over in stressed cells, albeit with an increased half-life of 40 min. A model can now be proposed to explain how the turnover of this protein adapts in response to alterations in cellular redox state.

The Nrf2 transcription factor regulates many antioxidant and detoxification genes in response to oxidative insult (1–3). The resulting biochemical alterations enhance the capacity of cells to survive the stress by detoxifying the causative agent along with by-products of the stress, by repairing or recycling damaged macromolecules, and ultimately, restoring redox homeostasis. The pivotal role of Nrf2 in this adaptive response is clear from the lack of up-regulation of these genes in mice lacking this factor (4–7).

Induction of many genes in response to oxidative stress occurs through the antioxidant-response element (ARE)[1] (for a review, see Ref. 8). This enhancer is bound by "cnc" bZIP proteins, which consists of not only Nrf2 but also the p45 subunit of NF-E2, Nrf1, and Nrf3, and the more distantly related members Bach1 and Bach2. These proteins bind AREs as obligate heterodimers with any one of three small Maf proteins (MafF, MafG, and MafK), which may themselves also bind as homodimers (for a review, see Ref. 9). Furthermore, other bZIP proteins are reputed to bind this enhancer (9). The transcriptional state of ARE-regulated genes is determined by the identity of the dimer recruited. For example, small Maf homodimers, which lack transactivation domains, are not competent to drive transcription from this element (Ref. 10), and Bach1-containing heterodimers actively repress transcription (11). In comparison, Nrf2 has been shown to be a strong transactivator, and its recruitment to an ARE, as a heterodimer with a small Maf partner molecule, results in transcriptional up-regulation of the gene in question (1, 12). The existence of functionally distinct bZIP dimers allows the cell to control ARE-driven gene transcription by varying the quantity of specific cnc and small Maf proteins in the nucleus and, therefore, the spectrum of dimers expressed. Accordingly, cellular adaptation to oxidative stress involves, among other changes, a rapid increase in the nuclear level of Nrf2 (13–15), possibly coupled with a decrease in the amount of Bach1 (16), leading in turn to enhanced recruitment of Nrf2-containing dimers to the promoters of ARE-regulated genes (17).

The amount of Nrf2 protein in the nucleus is controlled by the cytoplasmic, actin-bound protein, Keap1 (Kelch-like ECH-associated protein 1). ECH (erythroid cell-derived protein with cnc homology) is a synonym for *Gallus gallus* Nrf2. This Kelch-repeat protein was originally identified because it can interact with the N-terminal Neh2 (Nrf2-ECH homology 2) domain of Nrf2. Subsequently, Keap1 was found to bind directly to Nrf2 via an ETGE tetrapeptide motif within Neh2 (18–19). Initial overexpression assays indicated that Keap1 dictates the subcellular localization of Nrf2. It was demonstrated to tether Nrf2 in the cytoplasm of homeostatic cells, but during oxidative stress this interaction was antagonized, leaving Nrf2 free to translocate to the nucleus (18).

* This work was supported by the Association for International Cancer Research Grant 03-074 and the World Cancer Research Fund Grant 2002/55. The costs of publication of this article were defrayed in part by the payment of page charges. This article must therefore be hereby marked "*advertisement*" in accordance with 18 U.S.C. Section 1734 solely to indicate this fact.

[S] The on-line version of this article (available at http://www.jbc.org) contains Supplemental Figs. 1–4.

§ To whom correspondence should be addressed: Biomedical Research Centre, Ninewells Hospital and Medical School, Dundee DD1 9SY, Scotland, UK. Tel.: 0044-1382-660111; Fax: 0044-1382-669993; E-mail: m.j.m.mcmahon@dundee.ac.uk.

[1] The abbreviations used are: ARE, antioxidant response element; BTB, Broad-complex, Tramtrack, and Bric-a-brac; CHX, cycloheximide; cnc, cap 'n collar; ER, endoplasmic reticulum; HA, hemagglutinin; Keap1, Kelch-like ECH-associated protein 1; Neh, Nrf2-ECH homology; Nrf, NF-E2-related factor; Sul, sulforaphane; Ubl, ubiquitin-like; E1, ubiquitin-activating enzyme.

Recent studies (13–15, 20–21) indicate that oxidative stress influences not only the subcellular distribution of Nrf2 but also the total amount of Nrf2. Thus, in the nontransformed RL34 rat liver epithelial cell line, rNrf2 protein was undetectable under homeostatic conditions, but levels of the protein increased rapidly in the nucleus following treatment with sulforaphane (Sul), a model oxidative stressor (15). To account for these findings, it has been proposed that Keap1 both sequesters Nrf2 in the cytoplasm and enhances proteasomal degradation of the transcription factor in homeostatic cells (14, 15). Consistent with this model, we have demonstrated previously in COS1 cells that both the steady-state level of Nrf2 protein and its half-life are redox-sensitive, when coexpressed with Keap1. Deletion of the ETGE tetrapeptide motif from the Neh2 domain of Nrf2 demonstrated that its redox-sensitive interaction with Keap1 underpins its decreased stability during homeostatic conditions (15). To our surprise, although interaction with Keap1 enhanced the rate of proteasomal degradation of Nrf2 in homeostatic cells, the interaction did not enhance ubiquitination of the bZIP factor (15). Further examination of how the Neh2 domain controls protein half-life revealed that it does not simply contain the interaction site for Nrf2 and Keap1 but that this region is a redox-sensitive degron. Specifically, when Neh2 was fused to Gal4 and coexpressed with Keap1, the half-life of the recombinant protein was reduced, and its steady-state level became redox-sensitive. Deletion of the ETGE motif from the fusion protein also showed that the Neh2 domain could mediate proteasomal degradation independently of its interaction with Keap1. We thus proposed that Nrf2 is capable of being degraded proteasomally, via its Neh2 degron, both dependently and independently of Keap1. Under homeostatic conditions, the Neh2 degron mediates a rapid, Keap1-dependent degradation of Nrf2 (15). By contrast, under conditions of oxidative stress, the Neh2 degron directs a less rapid, Keap1-independent degradation of the bZIP factor.

The relationship between Keap1-dependent and -independent Neh2-mediated degradation is unclear. It is not known whether Keap1 simply acts to enhance the rate of the Keap1-independent mechanism or whether several pathways for Nrf2 degradation exist.

Comparison of the amino acid sequence of SKN-1, a transcription factor in *Caenorhabditis elegans* that responds to oxidative stress, with that of Nrf2 has revealed the presence of a conserved peptide called the "DIDLID element" in the nematode protein (22). This element is located between residues 99 and 112 of SKN-1, whereas in mouse, rat, and human Nrf2 it resides in the Neh2 domain between amino acids 17 and 32 (Fig. 1). In SKN-1, the DIDLID element is part of a transactivation domain, although this property is also shared with other regions of the nematode factor. The function of the region in Nrf2 homologous to the SKN-1 DIDLID element is not known, but the striking conservation suggests it performs an essential role. Given the fact that Neh2 helps control the turn over of Nrf2, it is important to establish whether the Neh2 subdomain equivalent to the SKN-1 element contributes to this process. Besides Neh2, five additional domains, Neh1, Neh3, Neh4, Neh5, and Neh6, have been identified in Nrf2. It is not known if these regions contribute to the destabilization of the bZIP protein.

In this paper we report for the first time that ubiquitination of a Gal4(HA)mNeh2 fusion protein depends upon the subdomain equivalent to the DIDLID element in SKN-1. By deleting amino acids 17–32 from full-length mNrf2, we demonstrate that Keap1 functions to enhance the rate of degradation of Nrf2 by acting downstream of ubiquitination directed by the DIDLID element. Whereas the Neh2 domain is both necessary

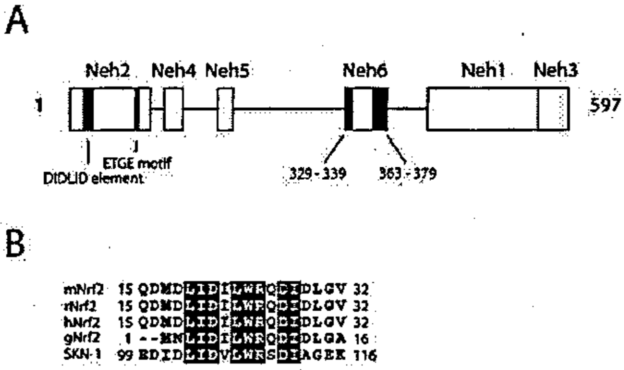

FIG. 1. **Structure of Nrf2.** *A*, schematic of the conserved domain structure of mouse Nrf2 based on a sequence alignment of orthologous Nrf2 proteins is presented. Conserved domains are referred to as Neh domains. The DIDLID element (amino acids 17–32) and the ETGE motif (amino acids 79–82) of the Neh2 domain are highlighted, as are two highly conserved regions of the Neh6 domain (amino acids 329–339 and 363–379). A complete sequence alignment of orthologous Nrf2 proteins from human to fish and a description of the known functions of the Neh domains can be found in the supplemental Fig. 1. *B*, a comparison of the regions of mouse (*m*), rat (*r*), human (*h*), and chicken (*g*) Nrf2 proteins encompassing DIDLID elements, and the corresponding sequence from *C. elegans* SKN-1 protein is presented. The sequence defined as the DIDLID element in SKN-1 is *underlined*. In the context of mNrf2, we use the term to refer to amino acids 17–32.

and sufficient for degradation of Nrf2 in homeostatic cells, it can be removed without altering the turnover rate of the protein in oxidatively stressed cells. Instead, degradation of the protein in stressed cells is predominantly mediated by the previously unrecognized, redox-insensitive Neh6 degron.

EXPERIMENTAL PROCEDURES

Plasmids—pCG-GAL(HA), which expresses a hemagglutinin (HA)-tagged GAL4 DNA-binding domain was a kind gift of Dr. William P. Tansey (Cold Spring Harbor Laboratory, NY) and has been described in Ref. 23. pCG-GAL(HA)mNeh6, which expresses Gal4(HA)mNeh6, a HA-tagged Gal4 DNA-binding domain fused to the Neh6 domain of mNrf2, was generated by PCR amplification of the region coding amino acids 318–401 by using the primer pair 5′-GACCTGTCACTGTCTAGAGCTTTCAACCCG-3′ and 5′-CATAGGAGCACTGGATCCTTGCTATGGTGACAGAGGCTG-3′. The resulting product was digested with XbaI and BamHI and ligated into similarly digested pCG-GAL(HA). pCG-GAL(HA)mNeh2, which expresses Gal4(HA)mNeh2, a hemagglutinin (HA)-tagged GAL4 DNA-binding domain-mNeh2 fusion protein, has been described previously, as has pcDNA3.1/V5mNrf2, which expresses full-length mNrf2 tagged at the C terminus with a V5 epitope (mNrf2-V5) (15). All constructs expressing the deletion mutants of Gal4(HA)mNeh2 or mNrf2-V5 mentioned in the text were generated from the above parental vectors by deletion mutagenesis using the GeneEditor kit (Promega). The sequences of the mutagenic oligonucleotides used are available on request. pcDNA3.1/V5HisCmKeap1 and pcDNA3.1/mKeap1, which express mKeap1-V5-hexahistidine and untagged mKeap1, respectively, have been described previously (15). The pARE-164CAT reporter construct was a gift from Dr. Cecil B. Pickett (Schering Plough Research Institute, Kenilworth, NJ) and has been described previously (24). pCMVβ-gal (Clontech) expresses β-galactosidase under the control of a cytomegalovirus promoter and was included in all transfections as an internal control. pHisUb, which expresses hexahistidine-tagged octameric ubiquitin precursor protein from a cytomegalovirus promoter (25), was provided by Prof. David P. Lane (University of Dundee). All constructs prepared for this study were sequence-verified.

Cell Culture, Transfections, Chemical Challenge, and Reporter Assays—ts20TG^R and H38.5 cells (26) were kind gifts from Profs. Harvey L. Ozer (University of Medicine and Dentistry of New Jersey-New Jersey Medical School) and Christoph Borner (Albert-Ludwigs University, Freiburg, Germany). The ts20TG^R cell line harbors a temperature-sensitive mutant E1 enzyme. The mutant enzyme permits growth at 34.5 °C but is inactivated by shifting cells to the nonpermissive temperature of 39 °C. This cell line was maintained at 34.5 °C in Dulbecco's modified Eagle's medium (Invitrogen) supplemented with 10% (v/v) heat-inactivated fetal calf serum (Invitrogen) and penicillin-streptomycin. The H38.5 cell line was derived from the ts20TG^R cell line and contains stably integrated DNA expressing the wild-type E1 protein. It was maintained as for the parent cell line, but its growth medium was supplemented with 50 μg/ml hygromycin B (Sigma) to maintain the integrated DNA. COS1 cells were grown in Dulbecco's modified Eagle's medium (Invitrogen) supplemented with 10% (v/v) heat-inactivated fetal calf serum (Invitrogen) and penicillin-streptomycin. RL34, non-transformed rat liver epithelial cells, were maintained in Dulbecco's modified Eagle's medium (Invitrogen) supplemented with 10% (v/v) heat-inactivated fetal calf serum (Invitrogen), 2 mM L-glutamine, and penicillin-streptomycin. Cells were seeded into either 6-well plates or 60-mm tissue culture dishes at least 18 h before transfection and were ~50% (ts20TG^R, H38.5, or RL34 cells) or 90% (COS1 cells) confluent at the time of transfection. Cells were transfected using either Lipofectin (COS1) or LipofectAMINE 2000 (ts20TG^R, H38.5, or RL34 cells) (both products from Invitrogen) according to the manufacturer's instructions. Cells were challenged with chemicals not less than 40 h after plating. Sul was obtained from LKT Laboratories. Cycloheximide (CHX) was from Sigma. MG132 was from Calbiochem. The β-galactosidase and chloramphenicol acetyltransferase reporter assays were carried out as described previously (15).

Whole-cell Extracts, In Vivo Ubiquitination Assay, Immunoprecipitation, and Immunoblots—For immunoblots, whole-cell lysates were prepared by scraping cell monolayers into ice-cold radioimmune precipitation assay buffer (50 mM Tris-Cl, pH 7.4, 150 mM NaCl, 1% (v/v) Nonidet P-40, 0.5% (w/v) deoxycholic acid, 0.1% (w/v) SDS supplemented with complete, EDTA-free protease inhibitor mixture (Roche Applied Science)). Lysates were clarified by centrifugation (16,000 × *g*, 15 min, 4 °C). The *in vivo* ubiquitination assay was carried out, and subsequently, whole-cell lysates and His-tagged proteins fractions were prepared as described previously (15) with the following modification: cells were not pretreated with MG132 before preparing whole-cell and His-tagged samples. Immunoprecipitation of HA-tagged proteins from clarified, whole-cell lysates was by conventional methods. Briefly, 50 μl of mouse IgG-agarose (Sigma) was washed with radioimmune precipitation assay buffer by repeated centrifugation (5,000 × *g*, 2 min, 4 °C), and the resin was mixed with and used to preclear the lysate, by end-over-end tumbling at 4 °C for 1 h. The suspension was centrifuged (5,000 × *g*, 2 min, 4 °C), and the precleared lysate was added to 50 μl of mouse anti-HA (clone HA-7)-agarose (Sigma) and washed as described above. This was incubated overnight at 4 °C with continuous end-over-end mixing. The following morning, the resin was washed with 3 volumes of radioimmune precipitation assay buffer by repeated centrifugation (5,000 × *g*, 2 min, 4 °C). Material that remained bound to the resin was eluted in 50 μl of Laemmli reducing sample buffer. Protein determination, SDS-PAGE, and immunoblotting were carried out as described previously (15). Antibodies used included a rabbit anti-mNrf2 serum (15), 1:10,000, mouse anti-V5 (Invitrogen), 1:2000, mouse anti-HA (clone 12CA5-Roche Applied Science), 0.4 μg/ml, rabbit anti-Gal4 serum (Upstate Biotechnology, Inc.), 1:2000, and a Goat anti-hKeap1 antibody preparation (Santa Cruz Biotechnology), 0.8 μg/ml.

RESULTS

The DIDLID Element in Nrf2 Is Essential for Keap1-independent, Neh2-mediated Degradation—In an attempt to define more clearly the relationship between Keap1-independent and -dependent Neh2-directed degradation, a region within the N-terminal domain of Nrf2 was sought that is required for its turnover in a Keap1-independent fashion. Within the first 96 amino acids, which define the Neh2 degron, two regions are highly conserved: amino acids 1–55 and 65–85 (see supplemental Fig. 1). On the basis of this information, we generated expression constructs for Gal4(HA)mNeh2$^{\Delta 1-16}$, Gal4(HA)mNeh2$^{\Delta 17-32}$, Gal4(HA)mNeh2$^{\Delta 33-55}$, and Gal4(HA)mNeh2$^{\Delta 65-85}$ to determine which of the four subdomains within Neh2 might be responsible for Keap1-independent turn over of Nrf2.

The steady-state expression levels of these proteins were initially compared with that of Gal4(HA)mNeh2. Untagged Keap1 was coexpressed with all proteins, but the degradation observed was Keap1-independent as the level of expression of the fusion proteins was sufficiently great to saturate the capacity of heterologously expressed mKeap1 to affect degradation (Fig. 8 in Ref. 15, see below also). Steady-state levels were measured using antibodies against the Gal4 DNA-binding domain, the HA tag, and mNrf2. All three reagents gave similar results (Fig. 2*A*).[2] The amount of both the Gal4(HA)mNeh2$^{\Delta 1-16}$ and Gal4(HA)mNeh2$^{\Delta 17-32}$ proteins was higher in COS1 cells than the other three fusion proteins, all of which accumulated to similar extents (Fig. 2*A*). The half-life of each protein in COS1 cells was determined by CHX chase assay (Fig. 2*B*). Gal4(HA)mNeh2, Gal4(HA)mNeh2$^{\Delta 33-55}$, and Gal4(HA)mNeh2$^{\Delta 65-85}$ all had statistically indistinguishable half-lives of ~1 h. The fact that deleting amino acids 65–85 (and thus the ETGE motif required for Keap1 binding) did not affect the half-life of the fusion protein demonstrated that the observed degradation is accomplished by a Keap1-independent mechanism. In stark contrast, deletion of amino acids 17–32 resulted in a protein of greatly enhanced stability. This protein had a half-life of ~8 h in COS1 cells, and it was effectively metabolically stable. This presumably accounts for the fact that it was observed to accumulate to a much higher steady-state level than the Gal4-wild-type Neh2 fusion protein from which it was derived. Finally, whereas deletion of amino acids 1–16 enhance the stability of the fusion protein, its half-life only extends from 1 to 2 h, which on its own cannot fully account for the large increase in its protein level when compared with that of the intact Neh2 fusion protein. This discrepancy has been observed consistently, and we speculate that it reflects some alteration in the rate at which conformationally mature Gal4(HA)mNeh2$^{\Delta 1-16}$ is generated. The stabilization achieved by deleting amino acids 1–16 is far more modest than that accomplished by deletion of amino acids 17–32. It appears likely that the modest increase in the half-life of Gal4(HA)mNeh2$^{\Delta 1-16}$ occurs because the ability of amino acids 17–32 to direct degradation of the fusion protein is impaired by deletion of amino acids 1–16.

The DIDLID Element Directs Polyubiquitination of Gal4(HA)mNeh2—Targeting of substrates to the 26 S proteasome generally requires prior polyubiquitination, although exceptions to this rule exist (27–29). Thus, one interpretation of the above results is that the DIDLID element is essential for polyubiquitination of the fusion protein, possibly by recruiting an ubiquitin ligase. Thus, we sought to compare, under steady-state conditions, the fractions of Gal4(HA)mNeh2$^{\Delta 17-32}$ and wild-type proteins that are conjugated to ubiquitin, utilizing the His-tagged ubiquitination assay of Treier *et al.* (25). COS1 cells were transfected with the plasmids indicated in Fig. 3*A*, and 24 h later, both the total amount of fusion protein in a whole-cell lysate and the amount of fusion protein recovered in the affinity-purified His-tagged fraction were determined by immunoblot analysis. Fusion protein recovered in the His-tagged fraction represents the polyubiquitinated form of the protein as no such protein was recovered in this fraction unless both fusion protein and His-tagged ubiquitin were coexpressed (Fig. 3*A*, *lanes 7–10*).

Although the absolute amount of ubiquitinated Gal4(HA)mNeh2$^{\Delta 17-32}$ recovered at steady-state was effectively identical to that of the wild-type Neh2-fusion protein, a greater amount of the DIDLID deletion mutant had to be expressed to "drive" ubiquitination to this extent (Fig. 3*A*, *cf. lanes 1* and *2* with *lanes 5* and *6*). By making serial dilutions of the whole-cell fraction, it was estimated that the DIDLID deletion mutant accumulated to approximately eight times the

[2] The inability of the rabbit anti-mNrf2 antiserum to effectively react with Gal4(HA)mNeh2$^{\Delta 65-85}$ appears to be due to the fact that the deleted region is immunodominant and not due to misfolding of the Neh2 region in its absence (M. McMahon and J. D. Hayes, unpublished observations).

A

B

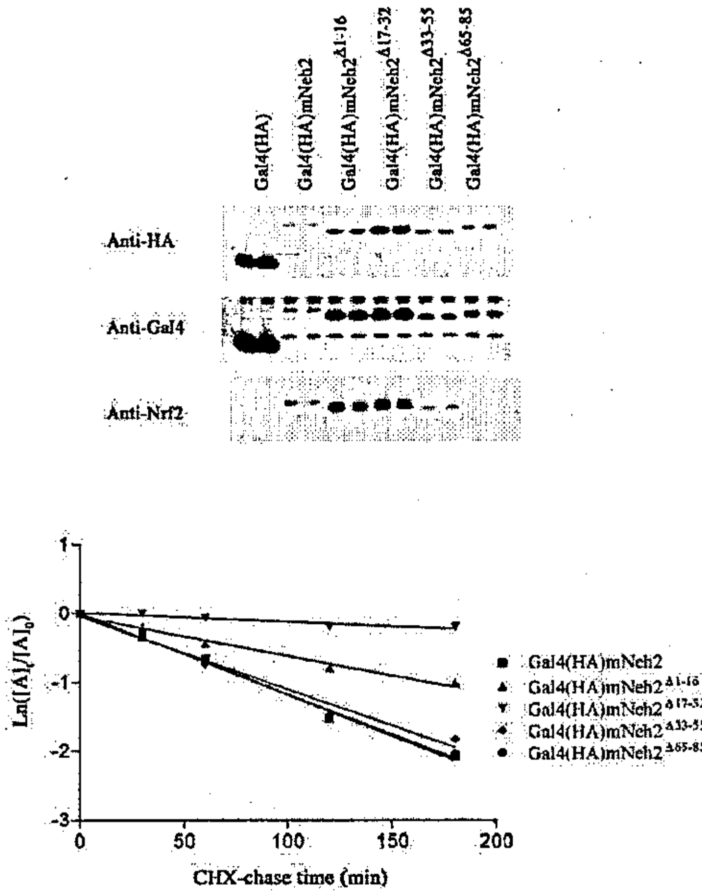

FIG. 2. **The DIDLID element is essential for Keap1-independent, Neh2-mediated degradation.** COS1 cells in 60-mm tissue culture dishes were transfected with 2 μg of a vector expressing either Gal4(HA), Gal4(HA)mNeh2, or various related deletion proteins as indicated in the figure. pcDNA3.1/mKeap1 (2 μg) was included in all transfection mixes as was 0.8 μg of pCMVβ-gal. *A*, whole-cell lysates were prepared from duplicate monolayers 24 h later, and the steady-state expression levels of the Gal4(HA) and related fusion proteins were determined by immunoblot analysis with the antibodies indicated to the *left* of each panel. *B*, CHX was spiked into each dish of cells to a final concentration of 40 μg/ml CHX. Subsequently, for each of the indicated fusion proteins, whole-cell lysates were prepared from transfected cells after the indicated CHX chase periods and probed with a mouse anti-HA antibody. The graph depicts the natural logarithm of the relative expression of each fusion protein (quantitated by densitometry) as a function of CHX chase time (mean of three independent experiments). The best fit line and the half-life, derived from the mean ± S.E. of the best-fit-line, are indicated for each fusion protein.

steady-state level achieved by the wild-type Neh2 fusion protein (data not shown). This is consistent with a prediction based on the magnitude of the increase in its half-life. Our interpretation of these experimental data is that both the wild-type and the DIDLID deletion fusion proteins are synthesized and fold correctly at the same rate. Therefore, at steady-state, both must be degraded at the same rate, and this explains the similarity in the absolute amount of these proteins found conjugated to ubiquitin. The increased total amount of fusion protein lacking Neh2 residues 17–32 arises because in the absence of the DIDLID element the rate of ubiquitination is reduced, and a greater cellular concentration of this fusion protein is required in order to achieve a similar cellular concentration of ubiquitinated material.

Given the fact that Gal4(HA)mNeh2$^{\Delta 1-16}$ is more stable than the wild-type fusion protein, we expected to find that its fractional ubiquitination was also less than that for Gal4(HA)mNeh2. Surprisingly, this does not appear to be the case (Fig. 3*A*, *cf. lanes 1* and *2* with *lanes 3* and *4*). By serial dilution, it was shown that the fractions of Gal4(HA)mNeh2 and Gal4(HA)mNeh2$^{\Delta 1-16}$ are essentially equivalent (supplemental Fig. 2). Furthermore, to check whether ubiquitination of Gal4(HA)mNeh2$^{\Delta 17-32}$ might be driven to some extent by the region of Neh2 encompassed by amino acids 1–16, we measured the fraction of Gal4(HA)mNeh2$^{\Delta 1-32}$ that was recovered conjugated to ubiquitin at steady state. The fraction of this protein that was ubiquitinated did not differ from the fraction measured for Gal4(HA)mNeh2$^{\Delta 17-32}$ (Fig. 3*B*, *cf. lanes 1* and *2* with *lanes 3* and *4*). Thus, deletion of amino acids 1–16 in Neh2 does not appear to compromise the capacity of the fusion protein to be ubiquitinated. The enhanced stability of the fusion protein attendant upon this deletion does not appear interpretable in terms of the conventional paradigm of proteasomal degradation. Perhaps, in some currently undefined fashion, this deletion affects not the rate of ubiquitination but rather the rate of degradation by the proteasome of the ubiquitinated substrate.

We also analyzed the fractional ubiquitination of Gal4(HA)mNeh2$^{\Delta 33-55}$, and it was identical to that of the wild-type fusion protein (data not shown). Unfortunately, although we can detect ubiquitinated fusion proteins with rabbit anti-Nrf2 serum, we cannot do so with the rabbit anti-Gal4 or mouse anti-HA reagents. We presume that ubiquitination occludes or modifies these regions of the fusion protein. As a consequence, this has precluded an analysis of the ubiquitin status of Gal4(HA) and Gal4(HA)mNeh2$^{\Delta 65-85}$.

The above results indicate that the DIDLID element in the Neh2 degron is necessary to allow efficient ubiquitination of Gal4(HA)mNeh2. Furthermore, the inverse correlation between the stabilities of Gal4(HA)mNeh2$^{\Delta 17-32}$ and Gal4(HA)mNeh2 and the extent to which they were ubiquitinated indicated that this type of modification was functionally important for Keap1-independent, Neh2-mediated proteasomal degradation. Nonetheless, the observation that a protein can be both proteasomally degraded and polyubiquitinated does not prove that a causal link exists between the two. For example, p21^{Cip1} is polyubiquitinated *in vivo* and is degraded by the proteasome, but mutants lacking lysine residues remain unstable (30). We therefore investigated whether polyubiquitination was necessary for degradation of Gal4(HA)mNeh2 by using the ts20TG^R cell line; these cells express a temperature-sensitive mutant E1 (ubiquitin-activating) enzyme, and at the nonpermissive temperature of 39 °C the enzyme is inactivated

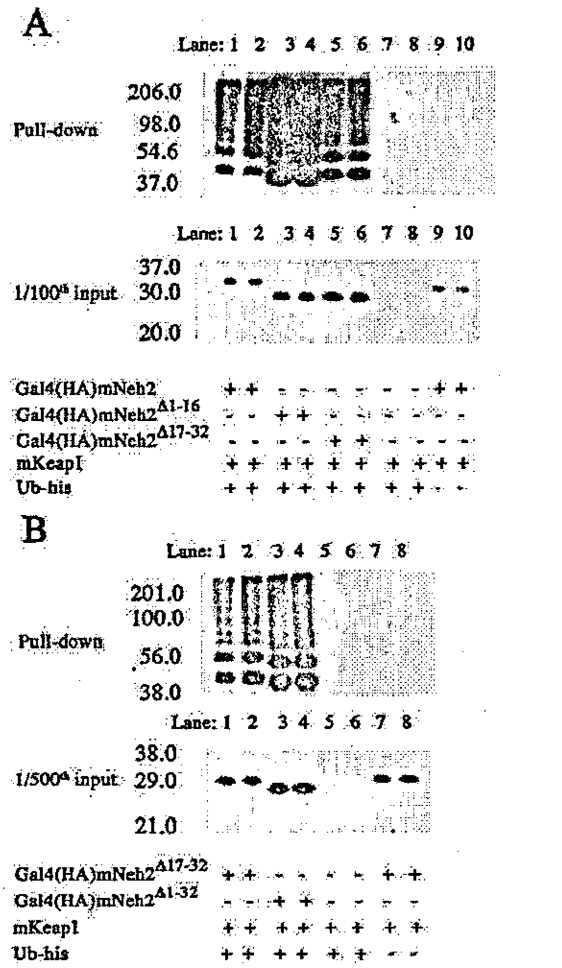

FIG. 3. **The DIDLID element directs polyubiquitination of Gal4(HA)mNeh2.** *A* and *B*, duplicate dishes of COS1 cells were transfected with the indicated plasmids. After transfection (24 h), a whole-cell lysate (input) and an affinity-purified His-tagged fraction (pull-down) were prepared from each dish of transfected cells and blotted with rabbit anti-mNrf2 serum. M_r markers are indicated to the *left* of each blot. *Ub*, ubiquitin.

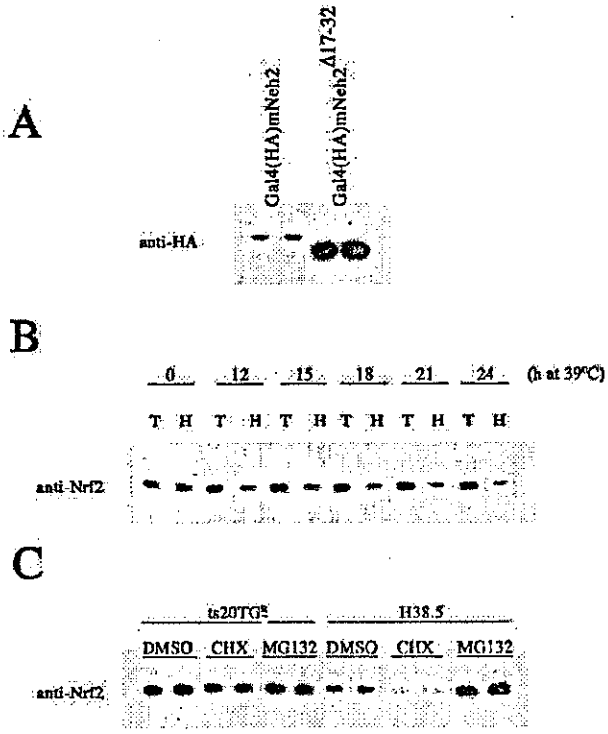

FIG. 4. **Polyubiquitination is essential for proteasomal degradation of Gal4(HA)mNeh2.** *A*, duplicate dishes of ts20TG^R cells were transfected with 2 μg of pcDNA3.1/mKeap1, 0.8 μg of pCMVβ-gal, and 2 μg of an expression vector for either Gal4(HA)mNeh2 or Gal4(HA)mNeh2$^{\Delta17-32}$, as indicated. After transfection (24 h), whole-cell lysates were prepared from each dish of cells and probed with mouse anti-HA. *B* and *C*, dishes of either ts20TG^R (T) or H38.5 (H) cells were transfected with 2 μg of pcDNA3.1/mKeap1, 0.8 μg of pCMVβ-gal, and 2 μg of an expression vector for Gal4(HA)mNeh2. *B*, dishes of cells were maintained at 34.5 °C and shifted to the nonpermissive temperature of 39 °C at such times that approximately 40 h after transfection they had been exposed to the nonpermissive temperature for the indicated times. At this point, whole-cell lysates were prepared from each dish of cells and blotted with rabbit anti-mNrf2. *C*, ~16 h after transfection, all dishes were shifted to the nonpermissive temperature of 39 °C for 15 h. Subsequently, duplicate dishes were treated with either 0.1% (v/v) Me_2SO (*DMSO*, vehicle), 40 μg/ml CHX, or 10 μM MG132 for 3 h, before whole-cell lysates were prepared from each dish of cells and probed with rabbit anti-mNrf2.

resulting in failure to covalently attach ubiquitin to proteins. The modes of degradation of Gal4(HA)mNeh2 appear to be similar in ts20TG^R and COS1 cells as deletion of the DIDLID motif resulted in a large increase in the steady-state expression level of the fusion protein in both cell lines (*cf.* Fig. 2*A* and Fig. 4*A*). When Gal4(HA)mNeh2 was heterologously expressed in ts20TG^R cells, and then transferred to 39 °C, the fusion protein did accumulate, albeit by a modest 3-fold (Fig. 4*B*). Nonetheless, in the control cell line, H38.5, derived from the ts20TG^R cell line but expressing wild-type E1 enzyme which maintains some activity at 39 °C, the Gal4(HA)mNeh2 protein failed to increase upon transfer to the nonpermissive temperature (Fig. 4*B*). It is therefore concluded that a functional ubiquitin-conjugating system is essential for efficient proteasomal degradation of Gal4(HA)mNeh2.

Subsequent experiments indicated that the modest increase in the level of the fusion protein was likely to be a consequence of a nonproteasomal mode of degradation of the fusion protein in ts20TG^R cells maintained at 39 °C. To test this hypothesis, Gal4(HA)mNeh2 was heterologously expressed in both the ts20TG^R and the H38.5 cell lines. The two cell lines were shifted to 39 °C for 15 h, and duplicate dishes of cells were treated with either vehicle (Me_2SO), translation inhibitor CHX, or the proteasomal inhibitor MG132 for a further 3 h. In the ts20TG^R cell line, treatment with MG132 did not lead to any accumulation of Gal4(HA)mNeh2 beyond that of Me_2SO-treated cells, suggesting that the inactivation of E1 was complete and no proteasomal degradation of Gal4(HA)mNeh2 occurred in this cell line at 39 °C (Fig. 4*C*). In comparison, accumulation of the fusion protein was evident in H38.5 cells upon treatment with MG132 (Fig. 4*C*). Despite the absence of detectable proteasomal degradation of Gal4(HA)mNeh2 in ts20TG^R cells at 39 °C, the 3-h CHX chase clearly resulted in a diminution in the amount of the protein. We attribute this to an unidentified, nonproteasomal degradation pathway.

The data presented above demonstrate that ubiquitination is essential for Keap1-independent, Neh2-mediated proteasomal degradation and that its DIDLID element is critical to ensure efficient ubiquitination.

Both the DIDLID Element and the ETGE Motif in Neh2 Are Essential to Confer Redox Sensitivity and Keap1 Dependence Upon the Half-life of Nrf2—Deletion of the DIDLID element from the Neh2 domain does not affect its capacity to interact with Keap1 because, by coimmunoprecipitation assay, we could

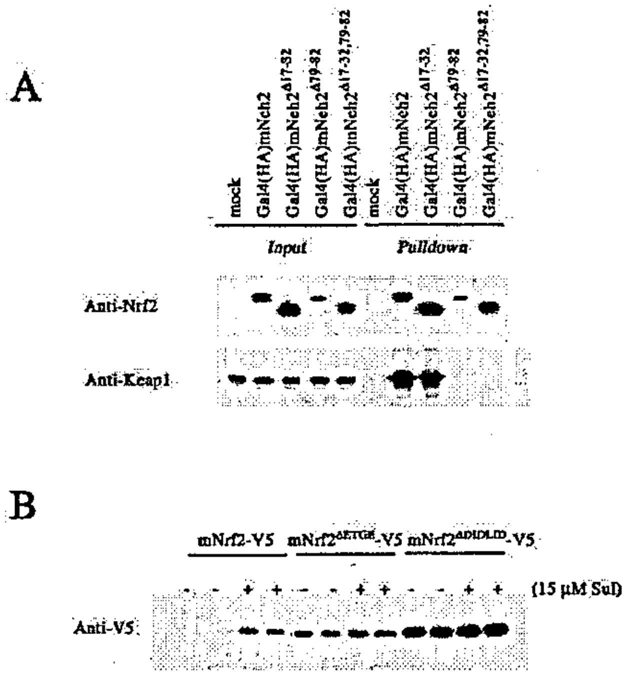

FIG. 5. **The DIDLID element does not influence the interaction of Nrf2 with Keap1.** *A*, COS1 cells in 60-mm dishes were either mock-transfected or transfected with vectors expressing the indicated fusion proteins, and 24 h later whole-cell lysates were prepared. To each of these lysates was added an equal volume of lysate from COS1 cells transfected with pcDNA3.1/V5HisCmKeap1. A portion of the lysate was kept as an input sample. HA-tagged material was immunoprecipitated from the remaining portion of each lysate. Both these *pull-down* fractions and *input* samples were probed by immunoblot with either rabbit anti-mNrf2, to detect the Neh2-fusion proteins, or with goat anti-hKeap1 to detect mKeap1-V5-hexahistidine. *B*, COS1 cells in 60-mm dishes were transfected with 2 μg of pcDNA3.1/mKeap1, 0.8 μg of pCMVβ-gal, and 2 μg of vector expressing either mNrf2-V5, mNrf2$^{\Delta ETGE}$-V5, or mNrf2$^{\Delta DIDLID}$-V5. 24 h after transfection, duplicate dishes of cells were treated with either 0.1% (v/v) Me_2SO (−) or 15 μM Sul (+) for 1 h, at which point whole-cell lysates were prepared and probed with mouse anti-V5 by immunoblot.

demonstrate that Gal4(HA)mNeh2$^{\Delta17-32}$ can interact with mKeap1 in cell lysates (Fig. 5*A*). It was therefore possible to determine whether Keap1 required not only the ETGE motif in Neh2 but also the DIDLID element in order for it to destabilize Nrf2 in homeostatic cells.

We coexpressed mNrf2$^{\Delta DIDLID}$-V5 (mNrf2 lacking amino acids 17–32 and tagged at the C terminus with the V5 epitope) with untagged mKeap1 in COS1 cells, which were subsequently treated with vehicle or Sul for 1 h before preparing whole-cell lysates. The level of mNrf2$^{\Delta DIDLID}$-V5 expressed at steady-state was invariant between the homeostatic and stressed cells (Fig. 5*B*), suggesting that the DIDLID element is essential for Keap1 to enhance the turnover rate of Nrf2 in homeostatic cells and, by implication, that Keap1 functions as part of the same pathway operative for Keap1-independent, Neh2-mediated degradation. Under the same conditions, mNrf2-V5 was expressed at lower levels in homeostatic cells than in stressed cells, and as expected, this was Keap1-dependent as deletion of the ETGE motif, to generate mNrf2$^{\Delta ETGE}$-V5, resulted in a protein whose expression level was elevated compared with its wild-type counterpart in homeostatic cells; its expression level was not affected by treatment with Sul.

To verify that Keap1 cannot enhance the turnover of mNrf2$^{\Delta DIDLID}$-V5 in COS1 cells, we determined its half-life in the presence and absence of heterologous mKeap1, both under homeostatic conditions and in cells that had been treated with Sul for 2 h (Fig. 6, *E* and *F*). It is evident that the half-life of this protein was similar under all conditions tested. In particular, when coexpressed with mKeap1, mNrf2$^{\Delta DIDLID}$-V5 had a half-life in homeostatic COS1 cells of 38 min and a half-life of 41 min in cells pretreated with Sul for 2 h (Fig. 6*F*).

As expected, the half-life of mNrf2$^{\Delta ETGE}$-V5 was also independent of whether mKeap1 was coexpressed or absent and whether the cells were homeostatic or stressed. This protein had a half-life of ~30 min under all tested conditions (Fig. 6, *C* and *D*).

Keap1 was only able to destabilize mNrf2-V5 protein containing both the ETGE motif and the DIDLID element in homeostatic COS1 cells. In stressed COS1 cells heterologously expressing mNrf2-V5 only, the half-life of the bZIP protein was 30 min, statistically indistinguishable from that of mNrf2$^{\Delta ETGE}$-V5 (Fig. 6, *A* and *C*). In homeostatic COS1 cells, however, the half-life of mNrf2-V5 was only 24 min (Fig. 6*A*). The reduced stability of mNrf2-V5, in the absence of heterologous mKeap1, in homeostatic COS1 cells is in agreement with our previous observation that the level of expression of tagged mNrf2 is enhanced by oxidative stress, even in the absence of heterologous mKeap1 (Ref. 15, Fig. 5*B*). It presumably reflects the presence of endogenous Keap1 in COS1 cells. Coexpression of mKeap1 with mNrf2-V5 further reduced the stability of the transcription factor in homeostatic cells. Under these conditions, mNrf2-V5 had a half-life of <7 min in homeostatic cells and a half-life of 38 min in stressed cells (Fig. 6*B*).

Two aspects of the data in Fig. 6 warrant further comment. First, the degradation of mNrf2-V5, when coexpressed with mKeap1, in homeostatic COS1 cells does not follow first-order kinetics. The quoted half-life was determined from an approximation of the initial rate of degradation at $t = 0$ min. As we could not model the curve using any common mathematical function, an initial "half-life" of 7 min was estimated from the slope of a line through the $t = 0$ and $t = 15$ min data points. A potential explanation for the observed kinetics of degradation is offered under "Discussion."

Second, the data suggest that not only does mKeap1 destabilize mNrf2-V5 in homeostatic COS1 cells, it might actually stabilize mNrf2-V5 in stressed cells. Thus, mNrf2-V5 expressed in stressed COS1 cells that lack heterologous mKeap1 has a half-life of 30 min. However, when mKeap1 is coexpressed with mNrf2-V5 in such cells, the half-life of the bZIP protein rises to 38 min (Fig. 6, *A* and *B*). No corresponding enhancement in half-life is observable for the mutant protein mNrf2$^{\Delta ETGE}$-V5 (Fig. 6, *C* and *D*). This effect of mKeap1 on the stability of mNrf2-V5 in stressed cells was found to be reproducible, although it is modest. This observation may not be of broad physiological relevance but may be related to limitations of the model system being investigated.

Collectively, these data support a model in which Keap1 destabilizes Nrf2 in homeostatic cells by directly interacting with the transcription factor through the ETGE motif, and thereby enhancing the rate of degradation mediated by the DIDLID element. Taken with our previous observation that mKeap1 does not influence the ubiquitination status of mNrf2-V5 under conditions where it does reduce its half-life (15), this suggests that Keap1 enhances the rate of Neh2-mediated degradation in homeostatic COS1 cells by acting downstream of ubiquitination mediated by the DIDLID element.

The Neh6 Domain Is a Redox-insensitive Degron, Which Is Essential for Degradation of mNrf2 in Oxidatively Stressed Cells—The fact that deletion of the DIDLID element only increased the half-life of mNrf2-V5 ~6-fold (from <7 min to ~40 min) was unexpected because deletion of this region from Gal4(HA)mNeh2 resulted in a fusion protein that was almost

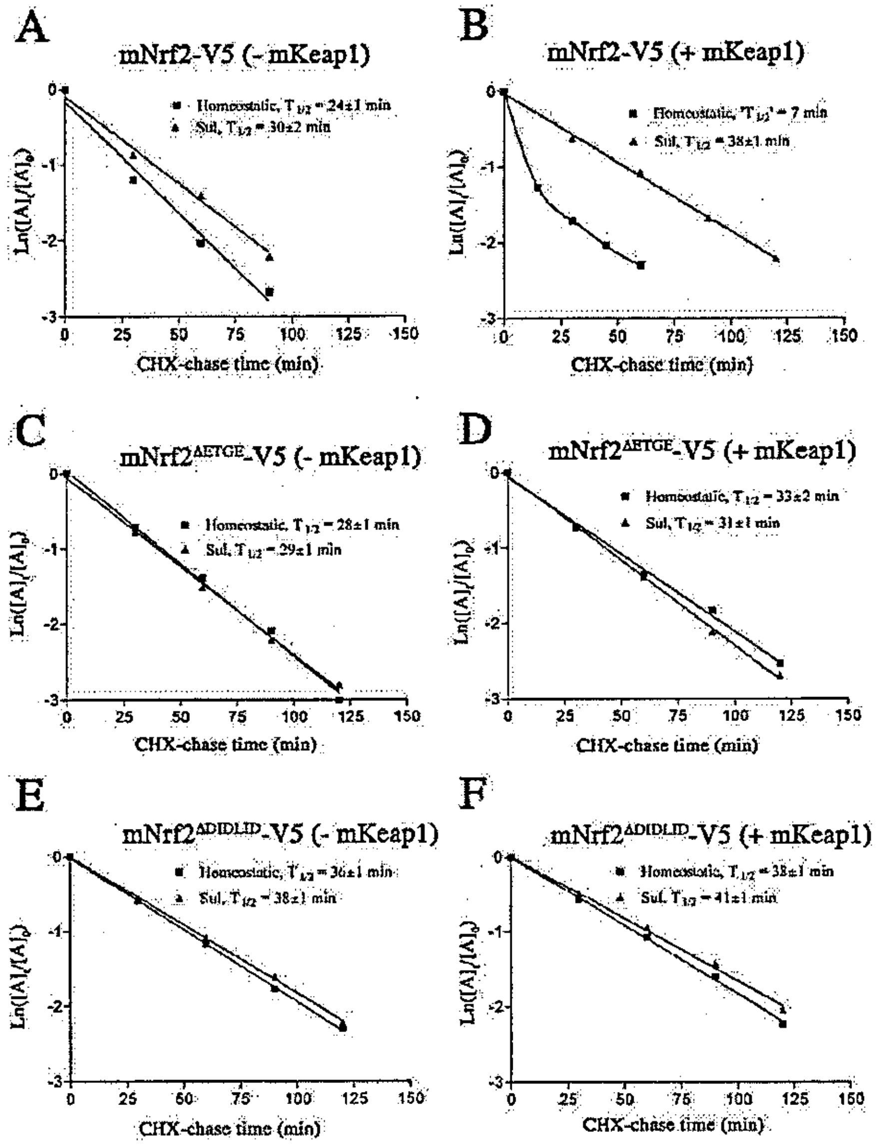

FIG. 6. **Both the DIDLID and the ETGE motifs of Nrf2 are essential to confer redox sensitivity upon Nrf2.** COS1 cells in 60-mm dishes were transfected with 2 μg of vector expressing either mNrf2-V5, mNrf2$^{\Delta ETGE}$-V5, or mNrf2$^{\Delta DIDLID}$-V5. Cells were cotransfected with 2 μg of either empty vector (*−mKeap1*) or vector expressing untagged mKeap1 (*+mKeap1*). pCMVβ-gal was included in all transfection mixes (0.8 μg) as an internal control. This gave six populations of cells differing in the proteins that they heterologously expressed (*A–F*). 24 h after transfection, cells were treated with either 0.1% (v/v) Me_2SO (homeostatic) or 15 μM Sul for 2 h before CHX was spiked into each dish to a final concentration of 40 μg/ml. Subsequently, whole-cell lysates were prepared at different time points and probed with mouse anti-V5. Each graph depicts the natural logarithm of the relative expression of V5-tagged protein as a function of CHX chase time in both homeostatic and stressed COS1 cells (mean of between two to four independent experiments). The best fit line and half-life, derived from the mean ± S.E. of the slope of the best fit line, are presented.

completely stable in COS1 cells. Furthermore, deletion of essentially the entire Neh2 domain from mNrf2-V5, to generate mNrf2$^{\Delta 3-85}$-V5, yielded a protein that had a half-life of only 37 min (Fig. 7*A*). These results suggested that Neh2 is not the sole degron in mNrf2, and two further points were evident. First, the second degron(s) was redox-insensitive as the half-life of mNrf2$^{\Delta DIDLID}$-V5 was not altered by treatment of COS1 cells with Sul (Fig. 6, *cf. E* and *F*). Second, the sole presence of the second degron(s) was sufficient to dictate the turnover rate of the transcription factor in oxidatively stressed COS1 cells. Thus while the Neh2 degron confers instability on the protein in homeostatic cells, it could be inactivated without impacting on the half-life of the protein in stressed cells. For example, mNrf2-V5, coexpressed with mKeap1 in stressed COS1 cells, had a half-life of 38 min, nearly identical to the half-life of mNrf2$^{\Delta DIDLID}$-V5 under similar conditions (Fig. 6, *cf. B* with *F*).

To delineate the region of Nrf2 required for its instability in stressed cells, we initially focused on Neh4 and Neh5 (amino acids 116–131 and 177–193, respectively, see supplemental Fig. 1) because they have been reported as transactivation domains (31), and such regions are occasionally coincident with degrons (23). To investigate Neh4 and Neh5, constructs expressing mNrf2$^{\Delta DIDLID,\Delta 116-131}$-V5 and mNrf2$^{\Delta DIDLID,\Delta 177-193}$-V5 were generated. Furthermore, the Neh6 domain was examined similarly, because it is a region of the protein that has had no function ascribed to it to date. As two particular regions within the Neh6 domain

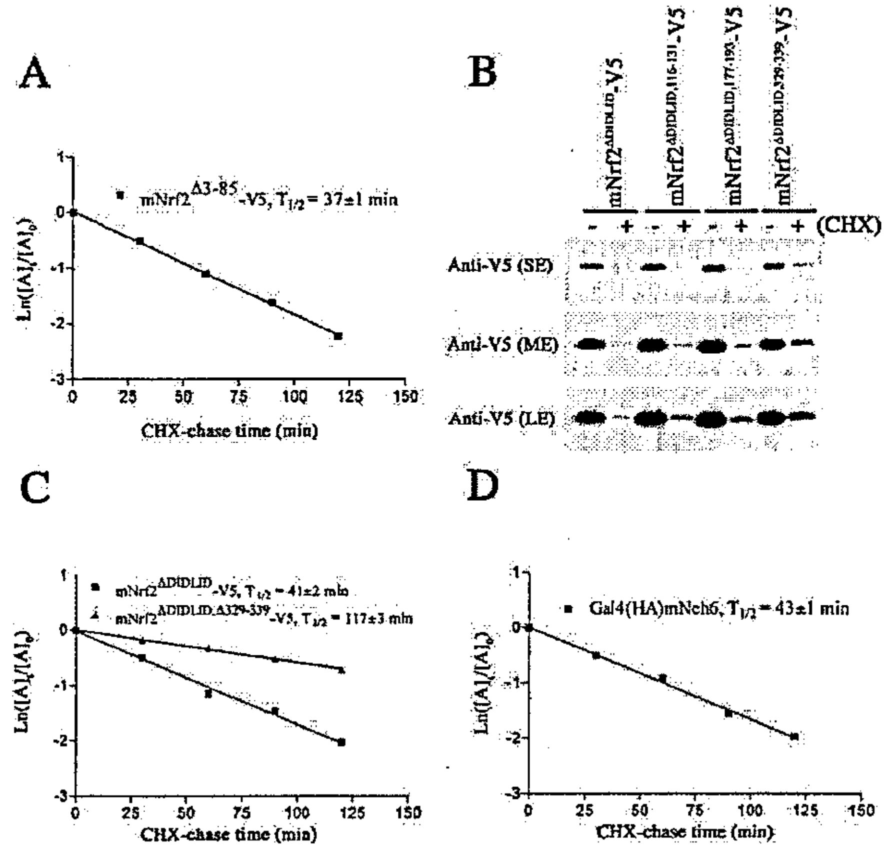

FIG. 7. **The Neh6 domain is a redox-insensitive degron.** *A*, COS1 cells in 60-mm dishes were transfected with 2 μg of a vector expressing mNrf2$^{\Delta 3-85}$-V5, 2 μg of pcDNA3.1/mKeap1, and 0.8 μg of pCMVβ-gal. 24 h after transfection, CHX was added to a final concentration of 40 μg/ml, and whole-cell lysates were prepared at different time points and probed with mouse anti-V5. The graph depicts the natural logarithm of the relative expression of mNrf2$^{\Delta 3-85}$-V5 as a function of CHX chase time (mean of two independent experiments). The best fit line and the derived half-life are depicted. *B*, COS1 cells in 60-mm dishes were transfected with 2 μg of vector expressing either of the four V5-tagged proteins indicated, 2 μg of pcDNA3.1/mKeap1, and 0.8 μg of pCMVβ-gal. 24 h later, cells were treated with either 0.1% (v/v) Me_2SO (−) or 40 μg/ml CHX (+) for 3 h before whole-cell lysates were prepared and probed with mouse anti-V5. *C* and *D*, COS1 cells in 60-mm dishes were transfected with 2 μg of pcDNA3.1/mKeap1, 0.8 μg of pCMVβ-gal, and 2 μg of vector expressing either one of the two indicated V5-tagged proteins (*C*) or Gal4(HA)mNeh6 protein (*D*). 24 h later, CHX was added to a final concentration of 40 μg/ml, and whole-cell lysates were prepared at different time points and probed with mouse anti-V5 (*C*) or rabbit anti-mNrf2 (*D*). The graphs depict the natural logarithm of the relative expression of the V5-tagged proteins (*C*) or Gal4(HA)mNeh6 as a function of CHX-chase time (mean of two independent experiments) (*D*). The best fit lines and the derived half-lives are presented.

are conserved (amino acids 329–339 and 363–379), constructs expressing mNrf2$^{\Delta DIDLID,\Delta 329-339}$-V5, mNrf2$^{\Delta DIDLID,\Delta 363-379}$-V5 and mNrf2$^{\Delta DIDLID,\Delta 329-379}$-V5 were generated.

Initially, we compared the fractions of mNrf2$^{\Delta DIDLID}$-V5, mNrf2$^{\Delta DIDLID,\Delta 116-131}$-V5, mNrf2$^{\Delta DIDLID,\Delta 177-193}$-V5, and mNrf2$^{\Delta DIDLID,\Delta 329-339}$-V5 remaining after a 3-h CHX chase (Fig. 7*B*). Deletion of the Neh4 or the Neh5 domains from mNrf2$^{\Delta DIDLID}$-V5 protein had no obvious effect on the stability of the protein in COS1 cells. In contrast, mNrf2$^{\Delta DIDLID,\Delta 329-339}$-V5 appeared more stable than mNrf2$^{\Delta DIDLID}$-V5, although it was still subject to degradation (Fig. 7*B*). A half-life for mNrf2$^{\Delta DIDLID,\Delta 329-339}$-V5 of 2 h was calculated compared with a half-life for mNrf2$^{\Delta DIDLID}$-V5 of 40 min (Fig. 7*C*). We initially suspected that the residual instability might stem from the remaining regions of the Neh6 domain. However, whereas mNrf2$^{\Delta DIDLID,\Delta 363-379}$-V5 and mNrf2$^{\Delta DIDLID,\Delta 329-379}$-V5 were more stable than mNrf2$^{\Delta DIDLID}$-V5, they were both of equal but not greater stability than mNrf2$^{\Delta DIDLID,\Delta 329-339}$-V5 (data not shown). These results suggested that the Neh6 domain constitutes a degron and that deletion of either amino acids 329–339 or amino acids 363–379 was sufficient to inactivate completely this degron. To formally demonstrate this, we generated a construct expressing a Gal4(HA)mNeh6 fusion protein. The fusion protein was immunoreactive with rabbit anti-Gal4 serum, mouse anti-HA, and rabbit anti-mNrf2 serum (data not shown). Its half-life was considerably shorter than Gal4(HA), being ~45 min (Fig. 7*D*). Taken in total, these findings demonstrate that in stressed COS1 cells, the Neh6 domain on its own is sufficient to account for the degradation rate of the transcription factor. The instability evident when the Neh6 degron is inactivated would appear to be physiologically relevant. We infer this from the fact that inactivation of the Neh6 degron does not compromise the functionality of mNrf2$^{\Delta DIDLID}$-V5 in a transactivation assay (supplemental Fig. 3) A trivial explanation invoking misfolding of the deletion proteins, for example, would therefore appear to be insufficient to explain the residual turnover of the transcription factor. This turnover is mediated by the proteasome (data not shown), but the region(s) of Nrf2 involved in the process have yet to be unidentified.

Finally, we demonstrated that the Neh6 degron is not only sufficient but is essential for efficient turnover of Nrf2 in oxidatively stressed COS1 cells. We generated a construct expressing mNrf2-V5 lacking amino acids 329–339

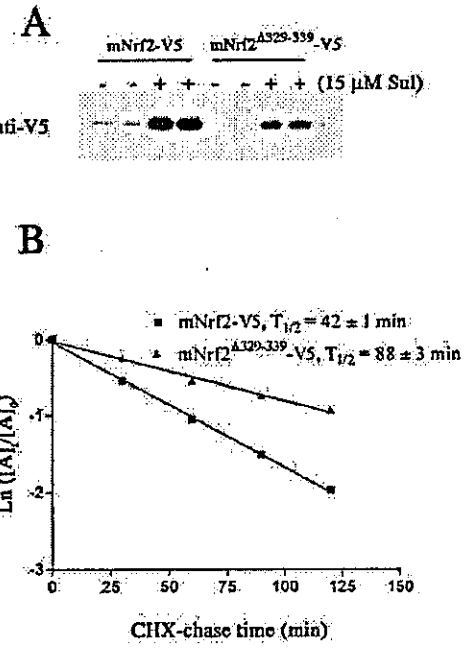

FIG. 8. **The Neh6 domain is essential for maximal turnover of Nrf2 in stressed cells.** COS1 cells in 60-mm dishes were transfected with 2 μg of a vector expressing either mNrf2-V5 or mNrf2$^{\Delta 329-339}$-V5, 2 μg of pcDNA3.1/mKeap1, and 0.8 μg of pCMVβ-gal. *A*, 24 h later, cells in duplicate dishes were treated with either 15 μM Sul (+) or vehicle (−) for 2 h, as indicated. *B*, 24 h later, CHX was added to a final concentration of 40 μg/ml, and whole-cell lysates were prepared at different time points and probed with mouse anti-V5. The graph depicts the natural logarithm of the relative expression of V5-tagged protein as a function of CHX-chase time (mean of two independent experiments). The best fit lines and derived half-lives are shown.

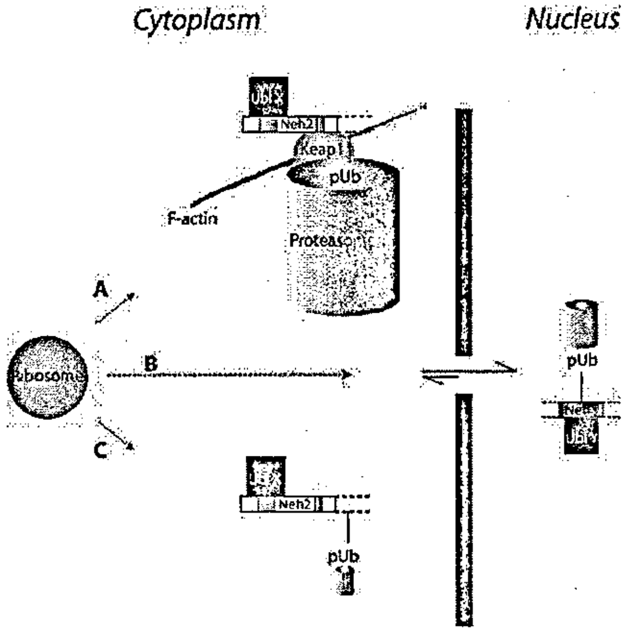

FIG. 9. **Degradation of Nrf2.** This schematic depicts the flux of Nrf2 throughout the cell. It is continuously synthesized in the cytosol by ribosomes at the ER, from where it is distributed, probably by both active and passive processes, to different regions of the cell. Continuously synthesized, it is also continuously degraded by mechanisms that vary with subcellular location. We hypothesize that at least three different spatially restricted pathways of degradation of Nrf2 may occur in cells. *A*, Keap1-dependent, DIDLID-directed degradation of Nrf2 occurs at the actin cytoskeleton. This is the most efficient mechanism for removing Nrf2, but only occurs in homeostatic cells as oxidative stress antagonizes the Nrf2-Keap1 interaction. *B*, Keap1-independent, DIDLID-directed degradation of Nrf2 occurs in the cytosol away from the actin cytoskeleton. *C*, Keap1-independent, Neh6-mediated degradation of Nrf2 occurs in the nucleus. Although less efficient than *A*, this is the predominant mode of degradation in oxidatively stressed cells. See text for further details. *Ubl X*, ubiquitin ligase recruited by the DIDLID element (shown in *green*); *Ubl Y*, ubiquitin ligase recruited by the Neh6 domain; *pUb*, polyubiquitin chain. The ETGE motif is shown in *pink*.

(mNrf2$^{\Delta 329-339}$-V5). When coexpressed with mKeap1, this protein was not impaired in its redox sensitivity. As with mNrf2-V5, it was expressed at very low levels in homeostatic cells, and its expression level was enhanced by treatment with Sul (Fig. 8*A*). However, when its half-life and the half-life of mNrf2-V5 were compared in COS1 cells after a 2-h exposure to Sul, its half-life was ~90 min, compared with 42 min for the wild-type protein (Fig. 8*B*). Thus, while the presence of Neh2 can mediate some turnover of Nrf2 in oxidatively stressed COS1 cells, the Neh6 domain is essential for its efficient turnover.

DISCUSSION

In the present paper we demonstrate for the first time that the DIDLID element within Neh2 is essential for Keap1-dependent destabilization of Nrf2. Thus, both the DIDLID element and the ETGE motif, two separate subdomains within Neh2, are required for the rapid turn over of Nrf2 under normal homeostatic conditions. Furthermore, we report also for the first time that the Neh6 domain makes the major contribution to the turn over of the transcription factor under conditions of oxidative stress. Hence, it is now proposed that at least two domains in Nrf2, the redox-sensitive Neh2 and redox-insensitive Neh6 degrons, contribute to its degradation. Based on the experimental findings reported here and those elsewhere, a model involving both these degrons that accounts for the redox-regulated turn-over of Nrf2 protein is depicted in Fig. 9. The model is justified and outlined below.

Role of the DIDLID Element—Evidence from three different cell lines indicates that the DIDLID element is critical for the destabilizing activity of the Neh2 degron. Figs. 2 and 4 demonstrate that removal of this element enhances the stability of the Gal4(HA)mNeh2 fusion protein in both the COS1- and ts20TG^{R}-transformed cell lines. Most important, this phenomenon is not restricted to transformed cell lines as it is also observed in the nontransformed rat liver RL34 epithelial cell line (supplemental Fig. 4). We propose that this element destabilizes the fusion protein by recruiting a currently unidentified ubiquitin ligase to it. The supporting evidence for this mechanistic interpretation is compelling. First, the necessity to recruit a ubiquitin ligase activity to the fusion protein is indicated by the observation that its degradation is reliant upon an intact functional ubiquitin-conjugating system (Fig. 4). Second, the notion that amino acids 17–32 recruit such an activity is suggested by the observation that deletion of this element results in a reduction in the fraction of the fusion protein that is ubiquitinated at steady state (Fig. 3). This reduction cannot be explained as a consequence of removal of a ubiquitin attachment site, as this region does not contain a lysine residue. Also, alterations in the subcellular distribution of the fusion protein, consequent upon removal of the DIDLID element, cannot be invoked to explain the reduction as immunocytochemical studies indicate that no observable differences exist between the subcellular distribution of Gal4(HA)mNeh2 and Gal4(HA)mNeh2$^{\Delta 17-32}$. Both are predominantly nuclear proteins but with a minor albeit significant fraction evident in the cytosol (data not shown). Thus, the only reasonable explanation for these findings is that the DIDLID element recruits a ubiquitin ligase activity. Formal proof, however, awaits the purification and identification of the DIDLID-binding ubiquitin ligase activity. We propose that this ability to recruit a ligase activity underlies Neh2-mediated, Keap1-independent proteasomal degradation, and like this mode of degradation (15), it may occur constitutively and independently of the redox state of the cell.

Functional Significance of the Interaction between Neh2 and Keap1—We have demonstrated previously that the redox-sensitive protein turnover mediated by the Neh2 degron is a consequence of its direct, redox-sensitive interaction with the actin-bound (32)[3] protein Keap1. This interaction requires the presence of the ETGE tetrapeptide motif of the Neh2 domain and is abrogated by its deletion (15). The consequence of this interaction with Keap1 is that, in homeostatic cells and only homeostatic cells, the rate of degradation of both Nrf2 and Gal4(HA)mNeh2 is enhanced. Here we report for the first time that whereas the Nrf2-Keap1 interaction is necessary, it is not sufficient to increase the turnover rate of Neh2-mediated degradation. Removal of the DIDLID element maintains the interaction between the two proteins, but it does not result in an enhanced rate of degradation of Nrf2 (Figs. 5 and 6). We believe this is a consequence of the fact that Keap1 operates upon the DIDLID-directed degradation pathway and can only function in conjunction with the ubiquitin ligase activity.

In theory, Keap1 could influence the rate of Neh2-mediated degradation by enhancing the rate of ubiquitination, mediated by the DIDLID element, of the protein. This possibility seems unlikely as our previous experiments have indicated that the ubiquitination status of full-length, tagged mNrf2 in COS1 cells is not influenced by either the presence or absence of heterologous mKeap1, the deletion of the ETGE tetrapeptide, or treatment with Sul all under conditions where mKeap1 does influence its half-life (15). Alternatively, as pointed out by Pickart (33), the *in vivo* concentration of ubiquitinated protein can be sufficiently high that transfer of ubiquitinated substrates to the proteasome may be rate-limiting, and therefore altering the rate of transfer of a specific ubiquitinated substrate to the proteasome, relative to generic substrates, is another way of controlling its turnover rate. Although it is conceivable that recruitment by Keap1 of Nrf2 to the cytoskeleton suffices to enhance the transfer of the transcription factor to the proteasome, a biologically more interesting possibility is that Keap1 actually associates with the proteasome. Indeed, a large body of experimental evidence demonstrates that numerous proteins bind to the proteasome in order to modulate the rate at which specific substrates are transferred to it (reviewed in Ref. 34). These include proteins such as Ubl/Uba (ubiquitin-associated)-containing proteins, and ubiquitin ligases (34–36). Of greater relevance to this discussion is a group of miscellaneous proteins with no obvious connection to the ubiquitination system but that affect the degradation of specific proteins by interacting with the proteasome. The yeast protein Cic1 was originally identified in a yeast two-hybrid screen for proteins interacting with the $\alpha 4$ subunit of the yeast proteasome (37). It has no effect on the global rate of proteasomal degradation, but in its absence the rates of degradation of two specific substrates (the SCF subunits Cdc4 and Grr1) are retarded. However, it does not influence their ubiquitination status. Instead, it has been proposed to act as an adaptor between the relevant SCF complexes and the proteasome, thereby ensuring the preferential degradation of important regulatory proteins over the general population of ubiquitinated substrates (37). Gankyrin and Homer3A11 bind the S6 and S8 ATPase subunits, respectively, of the base of the 19 S regulator of the 26 S proteasome. As with Cic1, they have been postulated to enhance the rate of degradation of their interacting partners, such as retinoblastoma protein and metabotropic glutamate receptors, by enhancing substrate targeting to the proteasome (38–40).

By analogy with the above examples, we propose that Keap1 increases the rate of transfer of ubiquitinated Nrf2 to the proteasome above the rate observed for the general population of ubiquitinated substrates by associating with the proteasome. It should be noted that there is a precedent for binding of Kelch-repeat proteins to the proteasome. Vidal and co-workers (41) screened a *C. elegans* cDNA library by yeast two-hybrid analysis by using 30 26 S proteasome subunits as bait. One cDNA isolated, W02G9.2, encodes a member of the Kelch-repeat family and was found to interact with the α 2, 4, 5, and 6 proteasome subunits in independent screens. Like Keap1, this protein contains an N-terminal BTB domain and 6 Kelch motifs. These proteins are 28% identical and 44% similar. Of the 16 Kelch-repeat proteins encoded by the *C. elegans* genome (42), W02G9.2 is the second-most similar to Keap1. This sequence similarity suggests that both proteins may mediate similar protein-protein interactions.

Keap1 may destabilize Nrf2 by mechanisms other than that evident in COS1 cells. Although we find no evidence that Keap1 influences the ubiquitination status of Nrf2 under conditions where it destabilizes it, the work of Zhang and Hannink (43) strongly suggests that Keap1 may indeed do so, at least in certain cellular contexts. They have proposed that Keap1 acts as a ubiquitin ligase (43). This is in agreement with the recent observation by others that BTB domains recruit Cul3-based ubiquitin ligase activities (44–47). Thus, Keap1 may recruit Cul3 via its BTB domain and Nrf2 via one of its Kelch repeats. The differences between our results and those presented by Zhang and Hannink (43) presumably reflect differences in the proteome expressed, or its subcellular disposition, in our respective model systems. It will be of interest to determine whether Keap1 can function both to enhance the rate of degradation mediated by the DIDLID element and itself recruit a ubiquitin ligase under physiological conditions or whether one or the other predominates in different organ/cell types.

The Neh6 Degron—Inactivation of the Neh2 degron by deletion of the DIDLID element only modestly stabilized Nrf2. Indeed, under conditions of oxidative stress the absence of Neh2-mediated degradation was largely irrelevant from the point of view of turn over of Nrf2. We hypothesized that there must be another degron that controlled the rate of degradation of Nrf2 in stressed cells. The Neh6 domain was shown to be such a degron (Fig. 7). It should be noted that other regions also contribute to proteasomal degradation of Nrf2 as inactivation of both the Neh2 degron and the Neh6 degron still left a protein with a half-life of 2 h. Although little is known about Neh6 at present, our data support the following two observations. First, Keap1 is incapable of enhancing the rate of degradation mediated by this degron. Thus mKeap1 can interact with mNrf2$^{\Delta 17-32}$-V5, but cannot influence its half-life in homeostatic cells (Fig. 6). Second, the presence of the Neh6 degron is essential for maximal turnover of the transcription factor in oxidatively stressed COS1 cells (Fig. 8). This is despite the fact that, at least in the context of Gal4(HA) fusion proteins, there is not any great difference in the efficiency of degradation mediated by the DIDLID element or the Neh6 domain (*cf.* Fig. 2 with Fig. 7).

Degradation of the Nrf2 Transcription Factor—We now present the broad outlines of a model accounting for the degradation of the Nrf2 transcription factor (Fig. 9). This model accommodates the following facts: Keap1 does not influence the rate of degradation directed by the Neh6 degron, the DIDLID ele-

[3] M. McMahon and J. D. Hayes, unpublished data.

ment does not make a major contribution to the degradation of Nrf2 in oxidatively stressed cells, and finally that the degradation of Nrf2 in homeostatic cells does not follow first-order kinetics. The salient features of this model are as follows.

(i) Keap1 contains reactive cysteine residues, and in oxidatively stressed cells these are modified leading to a conformational change that prevents its interaction with Nrf2 (48). Under such conditions, Keap1 cannot bind to and enhance the transfer of ubiquitinated Nrf2 (directed by the DIDLID element) to the proteasome. Nor can the modified Keap1 passively bind to nonubiquitinated Nrf2. In fact, in stressed cells Nrf2 is exclusively nuclear (15). Such a location reduces the opportunity for DIDLID-directed ubiquitination of Nrf2 (see point ii, below). As a result, in stressed cells Nrf2 is subjected primarily to Neh6-mediated degradation. We hypothesize that the Neh6 degron is functional only in the nucleus probably due to the fact that the proteins required for this function (presumably a ubiquitin ligase activity) are restricted to this compartment. As Keap1 is restricted to the cytoplasm, this provides a simple explanation for the observation that Keap1 cannot enhance degradation mediated by the Neh6 domain.

(ii) In homeostatic cells, Keap1 enhances the rate of DIDLID-directed degradation of Nrf2 by enhancing the rate of transfer of its polyubiquitinated form to a subset of proteasomes defined by the presence of an associated Keap1 protein(s). In some cell types, Keap1 may also enhance the rate of ubiquitination of Nrf2 in homeostatic cells via an associated ubiquitin ligase activity, most likely a Cul3-based ligase, recruited via the BTB domain. As Keap1 is restricted to the actin cytoskeleton, we infer that the putative ubiquitin ligase recruited by the DIDLID element must have access to this region of the cell. Although it is not necessary that the ubiquitin ligase is exclusively associated with the cytoskeleton, we suggest that it is excluded from the nucleus. Given that Nrf2 is predominantly nuclear in stressed cells, this would explain why the DIDLID element plays no major role in the turnover of Nrf2 in stressed cells.

(iii) As Keap1 is spatially restricted to the actin cytoskeleton, Keap1-dependent degradation must also be so restricted. On the basis of data in this paper, we postulate that both Keap1-dependent and Keap1-independent degradation occur simultaneously in different regions of homeostatic cells. The results presented in Fig. 6*B* suggests that degradation of mNrf2-V5 in homeostatic cells follows biphasic kinetics. The second phase of degradation is slower than the first and is indistinguishable from Keap1-independent degradation kinetics. We do not believe that this is coincidental. We propose that the biphasic degradation results from the superimposition of simultaneously operative Keap1-dependent and Keap1-independent degradation pathways in homeostatic cells, both pathways following first-order kinetics. The initial rapid degradation of Nrf2 after addition of CHX results from the predominance, initially, of Keap1-dependent degradation of Nrf2 in the vicinity of Keap1; during later times, as the concentration of Nrf2 in this region of the cell is reduced, Keap1-independent degradation of Nrf2 out with the environs of Keap1 predominates.[4] Unfortunately, the low level of mNrf2-V5 in homeostatic COS1 cells has so far precluded an empirical determination of its distribution.

(iv) Finally, the ultrastructure of the cell may have one final consequence for Keap1-dependent degradation of Nrf2 in homeostatic cells. As there is a constant flux of Nrf2 through the cell (it is constantly created and destroyed), kinetic factors become as important as thermodynamic factors in determining its ultimate fate. We are therefore intrigued by the observation of Diehl and co-workers (49) that Keap1 appears to colocalize with calreticulin, an endoplasmic reticulum (ER)-resident protein. Such a notion is not necessarily in conflict with the idea that Keap1 is actin-bound, as there is data in the literature suggesting an association between the architecture of the ER and the actin cytoskeleton (50–52). Protein synthesis does not occur uniformly throughout the cell but occurs primarily at the ER. The possibility exists that at least a portion of Keap1 might be coincident with the site of Nrf2 synthesis. Such a pool of Keap1 might be kinetically favored to interact with newly translated Nrf2. This may be important to ensure that Keap1-dependent degradation, the most efficient pathway of Nrf2 degradation, is predominant in homeostatic cells.

Although this model is speculative, particularly with regard to the influence of cell ultrastructure upon the rate of degradation of Nrf2, we believe it is both valid and useful. It is valid because it is sufficiently powerful to explain many of the features of Keap1-dependent regulation of Nrf2 that have been reported by us and other workers in the field, and it is useful because it provides a framework for the design of further experiments that in turn will cast light on the validity or otherwise of its basic tenets.

Concluding Comments—In this paper we have ascribed a function to the previously uncharacterized Neh6 domain. This domain appears to be specific to Nrf2 as BLAST searches have failed to identify its conserved primary sequences in other proteins. Of greater general interest perhaps, we have demonstrated that the DIDLID element is essential for the ubiquitination of Nrf2 and its rapid turn over during homeostatic conditions. This element can also be found in the related protein Nrf1, which also contains the ETGE motif, suggesting that at least some of the splice variants of this transcription factor are regulated in a similar fashion to Nrf2. Both Nrf1 and Nrf2 appear to be responsible for cellular adaptation to oxidative stress in vertebrates from human to fish (19, 53). In the more distantly related *C. elegans*, which belongs to a different metazoan clade from that of the vertebrates, adaptation to such stress relies upon the SKN-1 protein, which also contains a DIDLID element (54). Although we are unaware of any data pertaining to SKN-1 protein stability, this raises the intriguing possibility that redox-regulated transcription factor turn over is a mechanism of adaptation to oxidative stress that evolved early in the evolution of the metazoan lineage.

Acknowledgments—We are indebted to Profs. H. Ozer (University of Medicine and Dentistry of New Jersey) and C. Borner (University of Freiburg, Germany) for their gift of the ts20TG^R and H38.5 cells.

[4] We do not doubt the observation that both Keap1-dependent and -independent pathways of degradation occur simultaneously in our population of homeostatic COS1 cells nor the hypothesis that, given the ordered structure of the cell, both processes will occur simultaneously within the one cell. Nonetheless, it must be noted that our experimental strategy cannot distinguish between both pathways occurring intracellularly or, alternatively, occurring intercellularly. In particular, the transient transfection procedure will give rise to a heterogeneous population of cells possessing varying ratios of mKeap1 and mNrf2-expressing plasmids approximately in accordance with the binomial distribution. It is therefore possible that in some cells mNrf2-V5 cannot be degraded by a Keap1-dependent process. Also, it is unlikely that all cells in the population have the same redox potential as this characteristic varies with cell state. Therefore, some cells in the population are likely to experience oxidative stress even in the absence of Sul treatment.

REFERENCES

1. Itoh, K., Chiba, T., Takahashi, S., Ishii, T., Igarashi, K., Katoh, Y., Oyake, T., Hayashi, N., Satoh, K., Hayatama, I., Yamamoto, M., and Nabeshima, Y.-I. (1997) *Biochem. Biophys. Res. Commun.* 236, 313–322
2. McMahon, M., Itoh, K., Yamamoto, M., Chanas, S. A., Henderson, C. J., McLellan, L. I., Wolf, C. R., Cavin, C., and Hayes, J. D. (2001) *Cancer Res.* 61, 3299–3307
3. Kwak, M.-K., Wakabayashi, N., Itoh, K., Motohashi, H., Yamamoto, M., and

Kensler, T. W. (2003) *J. Biol. Chem.* **278,** 8135–8145
4. Chan, K., and Kan, Y. W. (1999) *Proc. Natl. Acad. Sci. U. S. A.* **96,** 12731–12736
5. Aoki, Y., Sato, H., Nishimura, N., Takahashi, S., Itoh, K., and Yamamoto, M. (2001) *Toxicol. Appl. Pharmacol.* **173,** 154–160
6. Cho, H.-Y., Jedlicka, A. E., Reddy, S. P. M., Kensler, T. W., Yamamoto, M., Zhang, L.-Y., and Kleeberger, S. R. (2002) *Am. J. Respir. Cell Mol. Biol.* **26,** 175–182
7. Lee, J.-M., Shih, A. Y., Murphy, T. H., and Johnson, J. A. (2003) *J. Biol. Chem.* **278,** 37948–37956
8. Nguyen, T., Sherratt, P. J., and Pickett, C. B. (2003) *Annu. Rev. Pharmacol. Toxicol.* **43,** 233–260
9. Motohashi, H., O'Connor, T., Katsuoka, F., Engel, J. D., and Yamamoto, M. (2002) *Gene (Amst.)* **294,** 1–12
10. Motohashi, H., Katsuoka, F., Shavit, J. A., Engel, J. D., and Yamamoto, M. (2000) *Cell* **103,** 865–875, and references therein
11. Sun, Y., Hoshino, H., Takaku, K., Nakajima, O., Muto, A., Suzuki, H., Tashiro, S., Shibahara, S., Alam, J., Taketo, M. M., Yamamoto, M., and Igarashi, K. (2002) *EMBO J.* **21,** 5216–5224
12. Venugopal, R., and Jaiswal, A. K. (1996) *Proc. Natl. Acad. Sci. U. S. A.* **93,** 14960–14965
13. Kwak, M.-K., Itoh, K., Yamamoto, M., and Kensler, T. W. (2002) *Mol. Cell. Biol.* **22,** 2883–2892
14. Itoh, K., Wakabayashi, N., Katoh, Y., Ishii, T., O'Connor, T., and Yamamoto, M. (2003) *Genes Cells* **8,** 379–391
15. McMahon, M., Itoh, K., Yamamoto, M., and Hayes, J. D. (2003) *J. Biol. Chem.* **278,** 21592–21600
16. Suzuki, H., Tashiro, S., Sun, J., Satomi, S., and Igarashi, K. (2003) *J. Biol. Chem.* **278,** 49246–49253
17. Nioi, P., McMahon, M., Itoh, K., Yamamoto, M., and Hayes, J. D. (2003) *Biochem. J.* **374,** 337–348
18. Itoh, K., Wakabayashi, N., Katoh, Y., Ishii, T., Igarashi, K., Engel, J. D., and Yamamoto, M. (1999) *Genes Dev.* **13,** 76–86
19. Kobayashi, M., Itoh, K., Suzuki, T., Osanai, H., Nishikawa, K., Katoh, Y., Takagi, Y., and Yamamoto, M. (2002) *Genes Cells* **7,** 807–820
20. Stewart, D., Killeen, E., Naquin, R., Alam, S., and Alam, J. (2003) *J. Biol. Chem.* **278,** 2396–2402
21. Nguyen, T., Sherratt, P. J., Huang, H.-C., Yang, C. S., and Pickett, C. B. (2003) *J. Biol. Chem.* **278,** 4536–4541
22. Walker, A. K., See, R., Batchelder, C., Kophengnavong, T., Gronniger, J. T., Shi, Y., and Blackwell, T. K. (2000) *J. Biol. Chem.* **275,** 22166–22171
23. Salghetti, S. E., Muratani, M., Wijnen, H., Futcher, B., and Tansey, W. P. (2000) *Proc. Natl. Acad. Sci. U. S. A.* **97,** 3118–3123, and references therein
24. Favreau, L. V., and Pickett, C. B. (1991) *J. Biol. Chem.* **266,** 4556–4561
25. Treier, M., Staszewski, L., and Bohmann, D. (1994) *Cell* **78,** 787–798
26. Chowdary, D. R., Dermody, J. J., Jha, K. K., and Ozer, H. L. (1994) *Mol. Cell. Biol.* **14,** 1997–2003
27. Verma, R., and Deshaies, R. J. (2000) *Cell* **101,** 341–344
28. Asher, G., Lotem, J., Sachs, L., Kahana, C., and Shaul, Y. (2002) *Proc. Natl. Acad. Sci. U. S. A.* **99,** 13125–13130
29. Kalejta, R. F., and Shenk, T. (2003) *Proc. Natl. Acad. Sci. U. S. A.* **100,** 3263–3268
30. Sheaff, R. J., Singer, J. D., Swanger, J., Smitherman, M., Roberts, J. M., and Clurman, B. E. (2000) *Mol. Cell* **5,** 403–410
31. Katoh, Y., Itoh, K., Yoshida, E., Miyagishi, M., Fukamizu, A., and Yamamoto, M. (2001) *Genes Cells* **6,** 857–868
32. Kang, M.-I., Kobayashi, A., Wakabayashi, N., Kim, S.-G., and Yamamoto, M. (2004) *Proc. Natl. Acad. Sci. U. S. A.* **101,** 2046–2051
33. Pickart, C. M. (2000) *Trends Biochem. Sci.* **25,** 544–548
34. Hartmann-Petersen, R., Seeger, M., and Gordon, C. (2003) *Trends Biochem. Sci.* **28,** 26–31
35. Glockzin, S., Ogi, F.-X., Hengstermann, A., Scheffner, M., and Blattner, C. (2003) *Mol. Cell. Biol.* **23,** 8960–8969
36. Xie, Y., and Varshavsky, A. (2002) *Nat. Cell Biol.* **4,** 1003–1007
37. Jäger, S., Strayle, J., Heinemeyer, W., and Wolf, D. H. (2001) *EMBO J.* **20,** 4423–4431
38. Dawson, S., Apcher, S., Mee, M., Higashitsuji, H., Baker, R., Uhle, S., Dubiel, W., Fujita, J., and Mayer, R. J. (2002) *J. Biol. Chem.* **277,** 10893–10902
39. Rezvani, K., Mee, M., McIlhinney, J., and Mayer, R. J. (2003) *Biochem. Soc. Trans.* **31,** 470–473
40. Krzywda, S., Brzozowski, A. M., Higashitsuji, H., Fujita, J., Welchman, R., Dawson, S., Mayer, R. J., and Wilkinson, A. J. (2004) *J. Biol. Chem.* **279,** 1541–1545
41. Davy, A., Bello, P., Thierry-Mieg, N., Vaglio, P., Hitti, J., Doucette-Stamm, L., Thierry-Mieg, D., Reboul, J., Boulton, S., Walhout, A. J. M., Coux, O., and Vidal, M. (2001) *EMBO Rep.* **2,** 821–828
42. Prag, S., and Adams, J. C. (2003) *BMC Bioinformatics* http://www.biomedcentral.com/1471-2105/4/42
43. Zhang, D. D., and Hannink, M. (2003) *Mol. Cell. Biol.* **23,** 8137–8151
44. Pintard, L., Willis, J. H., Willems, A., Johnson, J.-L. F., Srayko, M., Kurz, T., Glaser, S., Mains, P. E., Tyers, M., Bowerman, B., and Peter, M. (2003) *Nature* **425,** 311–316
45. Xu, L., Wei, Y., Reboul, J., Vaglio, P., Shin, T.-H., Vidal, M., Elledge, S. J., and Harper, J. W. (2003) *Nature* **425,** 316–321
46. Geyer, R., Wee, S., Anderson, S., Yates, J., III, and Wolf, D. A. (2003) *Mol. Cell* **12,** 783–790
47. Furukawa, M., He, Y. J., Borchers, C., and Xiong, Y. (2003) *Nat. Cell Biol.* **5,** 1001–1007
48. Wakabayashi, N., Dinkova-Kostova, A. T., Holtzclaw, W. D., Kang, M.-I., Kobayashi, A., Yamamoto, M., Kensler, T. W., and Talalay, P. (2004) *Proc. Natl. Acad. Sci. U. S. A.* **101,** 2040–2045
49. Cullinan, S. B., Zhang, D., Hannink, M., Arvisais, E., Kaufman, R. J., and Diehl, J. A. (2003) *Mol. Cell. Biol.* **23,** 7198–7209
50. Boevink, P., Oparka, K., Santa Cruz, S., Martin, B., Betteridge, A., and Hawes, C. (1998) *Plant J.* **15,** 441–447, and references therein
51. Wöllert, T., Weiss, D. G., Gerdes, H.-H., and Kuznetsov, S. A. (2002) *J. Cell Biol.* **159,** 571–577, and references therein
52. Shimada, O., Hara-Kuge, S., Yamashita, K., Tosaka-Shimada, H., Yanchao, L., Yongnan, L., Atsumi, S., and Ishikawa, H. (2003) *Cell Struct. Funct.* **28,** 155–163, and references therein
53. Leung, L., Kwong, M., Hou, S., Lee, C., and Chan, J. Y. (2003) *J. Biol. Chem.* **278,** 48021–48029
54. An, J. H., and Blackwell, T. K. (2003) *EMBO J.* **17,** 1882–1893

The transcription factor NRF2 protects against pulmonary fibrosis

HYE-YOUN CHO,*,†,1 SEKHAR P. M. REDDY,* MASAYUKI YAMAMOTO,‡ AND STEVEN R. KLEEBERGER*,†

*Department of Environmental Health Sciences, The Johns Hopkins University Bloomberg School of Public Health, Baltimore, Maryland, USA; †Laboratory of Respiratory Biology, National Institute of Environmental Health Sciences, National Institutes of Health, Research Triangle Park, North Carolina, USA; and ‡Institute of Basic Medical Sciences and Center for Tsukuba Advanced Research Alliance, University of Tsukuba, Tennoudai, Tsukuba, Japan

To read the full text of this article, go to http://www.fasebj.org/cgi/doi/10.1096/fj.03-1127fje; doi: 10.1096/fj.03-1127fje

SPECIFIC AIMS

Molecular mechanisms of fibrosis are poorly understood, although reactive oxygen species (ROS) are thought to have an important role. The primary objective of this study was to determine whether NF-E2-related factor 2 (NRF2), a key transcriptional regulator for antioxidant response element (ARE) -mediated induction of cellular antioxidants and detoxifying proteins, protects against pathogenesis of pulmonary fibrosis. To test this hypothesis, we exposed mice with targeted deletion of *Nrf2* (ICR/Sv129-*Nrf2*$^{-/-}$) and wild-type (ICR/Sv129-*Nrf2*$^{+/+}$) mice to bleomycin and compared pulmonary injury and fibrotic responses.

PRINCIPAL FINDINGS

1. Effects of targeted disruption of *Nrf2* on lung injury and fibrosis phenotypes

Mice (male, 6–10 wk) were anesthetized with 1.39 mg ketamine and 0.22 mg xylozine in saline (0.1 mL, i.p.), and a single dose (1.5 or 3.2 U/kg) of bleomycin in saline (1.25 U/mL) was delivered by intratracheal instillation. An equivalent volume of saline was instilled in control mice of each genotype. A significantly greater increase (40%) in lung/body weight ratio (a parameter of lung edema and matrix deposition) was found in *Nrf2*$^{-/-}$ mice compared with *Nrf2*$^{+/+}$ mice 6 days after bleomycin (3.2 U/kg). Bleomycin (3.2 U/kg) significantly increased (33%) lung hydroxyproline content (a marker of collagen deposition) over *Nrf2*$^{-/-}$ vehicle controls; no changes were found in *Nrf2*$^{+/+}$ mice. The lower dose of bleomycin (1.5 U/kg) was used to investigate prefibrotic molecular and cellular events as well as time-dependent changes in pathology. Fourteen days after bleomycin (1.5 U/kg) instillation, a significantly greater loss of body weight was found in *Nrf2*$^{-/-}$ mice, relative to *Nrf2*$^{+/+}$ mice. Mean numbers of total cells, neutrophils, lymphocytes, and epithelial cells recovered in bronchoalveolar lavage fluid were significantly higher (~2 to 3-fold) in *Nrf2*$^{-/-}$ mice than in *Nrf2*$^{+/+}$ mice 14 days after low dose (**Fig. 1**) and 6 days after high dose bleomycin (data not shown). Compared with *Nrf2*$^{+/+}$ mice, lung collagen accumulation determined by Sirius red dye-collagen binding assay was significantly greater in *Nrf2*$^{-/-}$ mice 3, 7, and 14 days after bleomycin treatment. Statistically significant deposition of collagen in *Nrf2*$^{+/+}$ mice was found only at 14 days after bleomycin.

2. Effects of targeted disruption of *Nrf2* on pulmonary pathology

Histological staining (Sirius red/Fast green, H&E) of lung tissue sections indicated significant differences in progression of pulmonary injury, inflammation, and fibrosis between *Nrf2*$^{-/-}$ and *Nrf2*$^{+/+}$ mice (Fig. 2). Predominant histopathologic features of *Nrf2*$^{-/-}$ mice instilled with bleomycin (1.5 U/kg) included alveolar inflammation (principally neutrophils and lymphocytes), diffused fibrotic patch formation with collagen accumulation, hyperplastic and hypertrophic changes of epithelium lining alveoli, small bronchi, and terminal bronchioles. Fibrogenesis was observed primarily in alveolar interstitium adjacent to terminal bronchioles, and alveolar bronchiolization was distinct in areas undergoing severe fibrotic remodeling. Compared with *Nrf2*$^{-/-}$ mice, relatively mild inflammation and only focal fibrotic lesions were found in *Nrf2*$^{+/+}$ mice at 7 days. Persistent inflammation and abnormal lung architecture characterized by extensive fibroblast proliferation, alveolar bronchiolization, and collagen-stained matrix deposition was evident in *Nrf2*$^{-/-}$ mice 14 days after

[1] Correspondence: Laboratory of Respiratory Biology, NIEHS, NIH, Research Triangle Park, North Carolina 27709, USA. E-mail: cho2@niehs.nih.gov

0892-6638/04/0018-1258 © FASEB

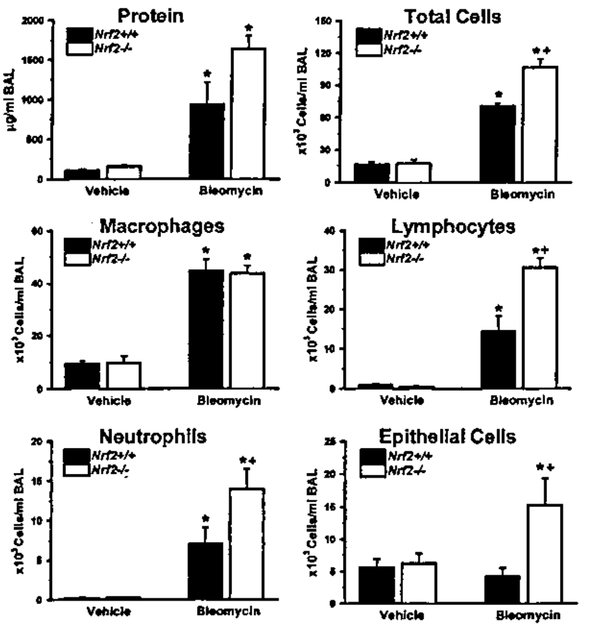

Figure 1. Effect of targeted disruption of *Nrf2* on bleomycin (1.5 U/kg)-induced increases in bronchoalveolar lavage phenotypes 14 days after instillation. Data are presented as means ± SEM (n=4–5/group). *Significantly different from genotype-matched vehicle control mice (P<0.05). +Significantly different from bleomycin-treated $Nrf2^{+/+}$ mice (P<0.05).

instillation. Fibrosis scoring by Ashcroft method ranging from 0 (no fibrosis) to 8 (total fibrosis) demonstrated that significant lung fibrosis was evident at 7 and 14 days postinstillation in both genotypes of mice. However, average fibrotic scores were significantly higher in $Nrf2^{-/-}$ mice compared with $Nrf2^{+/+}$ mice at 7 days (60%; 4.98±0.32 vs. 3.16±0.33) and 14 days (27%; 6.77±0.46 vs. 5.31±0.45) after bleomycin.

3. Bleomycin-Induced mRNA/Protein expression and transactivation of lung NRF2

Bleomycin caused significant time-dependent induction of NRF2 mRNA expression in lungs of $Nrf2^{+/+}$ mice (50% over saline controls at 14 days). Immunoblotting analyses detected marked bleomycin-induced increases of cytoplasmic and nuclear NRF2 accumulation in lungs of $Nrf2^{+/+}$ mice (14 days after instillation). Time-dependent increase of bleomycin-induced nuclear NRF2-DNA (NF-E2) binding activity was detected by gel mobility shift/supershift analysis in lungs of $Nrf2^{+/+}$ mice.

4. Effects of targeted disruption of *Nrf2* on bleomycin-induced antioxidant enzyme expression

Bleomycin caused up-regulation of mRNA for NAD-P(H):quinone oxidoreductase (NQO1), glutathione-S-transferase (GST)-Ya (α)/-Yp1 (pi)/-Yb1 (mu), catalytic (GLCLc) and regulatory (GLCLr) subunits of gamma glutamylcysteine ligase, thioredoxin reductase (TXNRD) 1, UDP glycosyl transferase 1a6, carboxylesterase (Ex), heme oxygenase (HO)-1, glutathione peroxidase (GPx) 2, and superoxide dismutase (SOD)-3 in $Nrf2^{+/+}$ mice over basal levels. Bleomycin-induced expression of all these genes was significantly higher in $Nrf2^{+/+}$ mice than in $Nrf2^{-/-}$ mice. Among these, mRNA levels of NQO1, TXNRD1, GLCLc, Ex, and GPx2 were constitutively attenuated in $Nrf2^{-/-}$ mice compared with $Nrf2^{+/+}$ mice, and their steady-state expression levels were not significantly altered by bleomycin instillation in $Nrf2^{-/-}$ mice. Consistent with gene expression results, bleomycin-induced protein levels of pulmonary GST-α, GST-mu, GPx, and HO-1 were significantly greater in $Nrf2^{+/+}$ mice than in $Nrf2^{-/-}$ mice, with peaks at 7 days. No statistically significant changes were detected in $Nrf2^{-/-}$ mice after bleomycin.

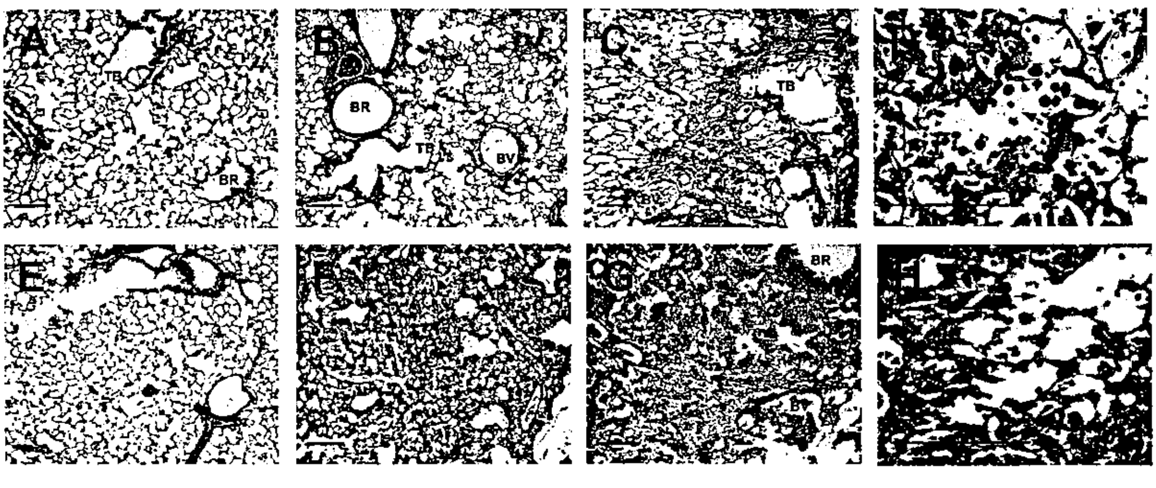

Figure 2. Differential progression of pulmonary injury and fibrosis in $Nrf2^{+/+}$ (*A–D*) and $Nrf2^{-/-}$ (*E–H*) mice after bleomycin (1.5 U/kg). Paraffin-embedded left lung tissue sections were processed for histological analyses and Sirius red/Fast green staining was performed to visualize collagen deposition (red dye staining) in control lungs (*A, E*) or fibrotic lung interstitium 7 (*B, F*) or 14 days (*C, G*) after bleomycin. Higher magnification of H&E-stained lung tissue sections illustrates alveolar bronchiolization in fibrotic lesions of $Nrf2^{+/+}$ (*D*) and $Nrf2^{-/-}$ (*H*) mice 14 days after bleomycin. Arrows, bronchiolization; TB, terminal bronchiole; BR, bronchiole; BV, blood vessel. Bar: 100 μm.

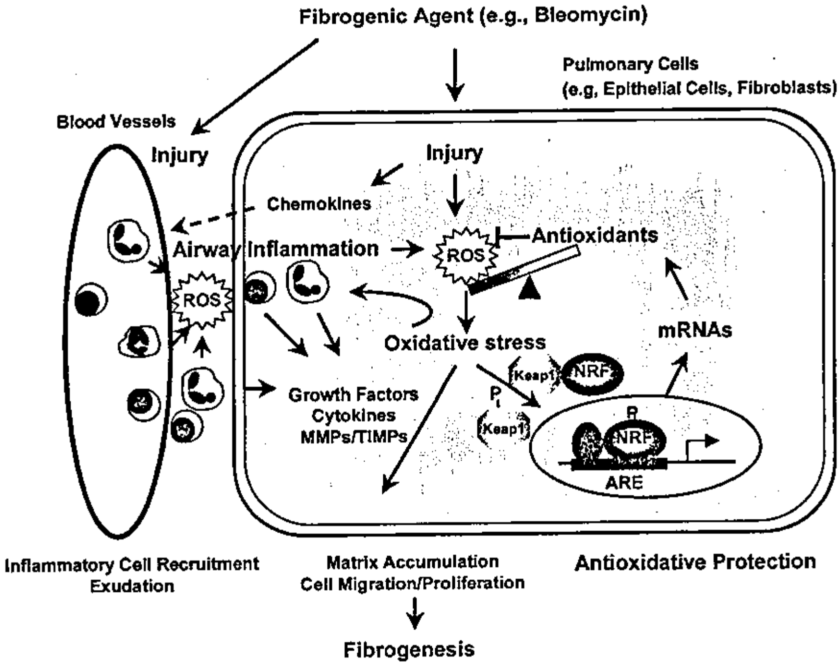

Figure 3. A hypothetical mechanism depicts a protective role of NRF2 in the pathogenesis of pulmonary fibrosis. Imbalance of cellular oxidant (ROS) and of antioxidant capacity induced by injury and inflammation causes oxidative stress in pulmonary cells. It may cause prefibrotic events (e.g., activation of growth factors) leading to matrix deposition and fibroblast proliferation. Oxidative stress may also trigger modification (e.g., phosphorylation) of Keap1-NRF2 sensor to release NRF2 from the complex. NRF2 binding to ARE in association with other transcription factor (e.g., small Maf, c-Jun) can induce transcriptional activation of antioxidant/detoxifying proteins to combat against ROS and further oxidative injury.

5. Effects of targeted disruption of *Nrf2* on bleomycin-induced lung injury/fibrosis marker expression

Greater accumulation of transcripts for several matrix markers of fibroproliferation (type 1 collagen α 2; Col1a2, fibronectin 1; FN1, tenascin-C) and pulmonary injury and remodeling markers (transforming growth factor-βs; TGF-βs, matrix metalloproteinases; MMPs, tissue inhibitor of metalloproteinase 1; TIMP1) was found in $Nrf2^{-/-}$ mice compared with $Nrf2^{+/+}$ mice after bleomycin. Transcripts of many of these genes were constitutively higher in $Nrf2^{-/-}$ mice than in $Nrf2^{+/+}$ mice, while tenascin-C and MMP7 were not detected in control lung tissues. Consistent with gene expression results, protein levels of lung MMP2, TGF-β, connective tissue growth factor (CTGF), and tenascin-C were significantly higher in $Nrf2^{-/-}$ mice than in $Nrf2^{+/+}$ mice after instillation (7 or 14 days postinstillation).

CONCLUSIONS AND SIGNIFICANCE

Results of the present study supported the hypothesis that NRF2 is protective against fibrotic lung injury. Relative to $Nrf2^{+/+}$ mice, targeted deletion of *Nrf2* significantly enhanced susceptibility to murine pulmonary inflammation and fibrosis induced by the anti-neoplastic drug bleomycin. Suppressed induction of NRF2-dependent antioxidant/defense enzymes in lungs of $Nrf2^{-/-}$ mice suggests that these enzymes may contribute to NRF2-mediated protection against bleomycin-induced lung fibrosis. This is the first study to suggest an upstream regulatory mechanism of cellular antioxidant enzyme defense in an experimental fibrosis model.

Fibrosis is an increasingly prevalent disorder, and is an end-state process in a number of chronic diseases of kidney, liver, and lung. In particular, idiopathic pulmonary fibrosis is a progressive and usually fatal disease of unknown etiology with no known effective therapy. A role for oxidants in the pathogenesis of pulmonary fibrosis has been suggested in previous studies. Protective roles of antioxidative mechanisms in pulmonary fibrosis were demonstrated by examining the role of enzymatic (e.g., SODs) or nonenzymatic (e.g., N-acetylcysteine) antioxidants. The thiol redox system (glutathione, thioredoxin) was also determined to be protective against lung fibrosis. The present study supports this concept, and provides a novel molecular mechanism through which antioxidative protection against fibrogenesis may occur. It is, however, important to note that antioxidative mechanism mediated by ARE-NRF2 response was not sufficient to completely ameliorate inflammation and fibrotic responses to bleomycin. Other antifibrotic mechanisms (e.g., interleukins-9 and 12) may interact for protection against fibrosis.

The present study demonstrated that bleomycin caused increased mRNA expression, lung protein levels, and nuclear DNA binding of NRF2 in advance of the onset of pulmonary inflammation and fibrogenesis. As depicted in **Fig. 3**, our findings suggest that activation of NRF2 and ARE-mediated induction of antioxidant defense enzymes during pathogenesis of ROS-mediated fibrogenesis has a key role in combating ROS and suppression of fibrotic tissue injury. Results from the current study may have important implications for development of combined therapies for bleomycin-toxicity and idiopathic pulmonary fibrosis to complement anti-inflammation therapy, which is only effective in subsets of fibrosis patients. FJ

Available online at www.sciencedirect.com
SCIENCE @ DIRECT®
ELSEVIER
Biochemical and Biophysical Research Communications 320 (2004) 62–69
BBRC
www.elsevier.com/locate/ybbrc

MafT, a new member of the small Maf protein family in zebrafish☆

Yaeko Takagi, Makoto Kobayashi,* Li Li, Takafumi Suzuki, Keizo Nishikawa, and Masayuki Yamamoto

ERATO-JST, Center for TARA and Institute of Basic Medical Sciences, University of Tsukuba, 1-1-1 Tennodai, Tsukuba 305-8575, Japan

Received 2 April 2004
Available online 7 June 2004

Abstract

Small Maf proteins play critical roles on morphogenesis and homeostasis through associating with CNC proteins. To date, three small Maf proteins, MafF, MafG, and MafK, have been reported in vertebrates, which share redundant functions. In this study, we tried to identify and characterize small Maf proteins in zebrafish to elucidate their conservation and diversity in the fish kingdom. We identified homolog genes of MafG and MafK but not MafF in zebrafish, indicating the former two are conserved among vertebrates. In addition, a novel type of small Maf protein MafT was identified. MafT protein bound MARE sequence as a homodimer or heterodimers with zebrafish Nrf2 or p45 Nfe2. Co-overexpression of MafT and Nrf2 synergistically activated MARE-mediated gene expression in zebrafish embryos. These results indicated that MafT is a new member of small Maf proteins and involved in the Nrf2-dependent gene regulation in cellular defense system.

Keywords: Diethylmaleate; Heterodimer; Luciferase assay; Nrf2; p45; Nfe2; Phase 2 induction; Radiation hybrid mapping; Small Maf protein; Transcription; Zebrafish

The induction of phase 2 enzyme genes is an important regulatory response for cytoprotection against electrophilic insults and reactive oxygen species [1]. Expression of phase 2 detoxifying enzymes and antioxidant proteins is strongly induced upon exposure to low levels of electrophiles or oxidative stress. Activation of the cellular defense system by phase 2 inducers renders cells more resistant to the potential challenges of a subsequent stress. This coordinated response is regulated through a *cis*-acting element called the antioxidant responsive element (ARE) or electrophile responsive element (EpRE) within the regulatory region of each gene. Analysis of gene disruption in mice has revealed that the transcription factor Nrf2 plays central roles in the ARE/EpRE-mediated transcriptional induction [2,3].

Nrf2 belongs to the family of Cap'n'collar (CNC)-type basic region-leucine zipper (bZIP) proteins, which includes p45 NF-E2, Nrf1, Nrf3, Bach1, and Bach2 [4]. Activation of Nrf2 is regulated in several steps: nuclear translocation, protein stabilization, and DNA binding [5]. Keap1, a member of the Kelch family of proteins, regulates the former two steps [6,7]. In the absence of phase 2 inducers, Nrf2 associates with Keap1 in the cytoplasm and is rapidly degraded by the ubiquitin–proteasome pathway, but upon the addition of phase 2 inducers, Nrf2 is stabilized, translocates into nuclei, and conducts the activation of target gene transcription [6,8]. Control of DNA binding is also critical for the Nrf2 functions, since Nrf2 cannot bind to the ARE/EpRE as a monomer or a homodimer, but Nrf2 must heterodimerize with one of the small Maf proteins for DNA binding and transactivation [9,10].

Seven members of Maf proteins have been identified in vertebrates, which are divided into the large and small Maf subfamilies [4]. The large Maf proteins include c-Maf [11], MafB [12], Nrl [13], and L-maf/MafA/S-maf

☆ *Abbreviations:* ARE, antioxidant responsive element; bZIP, basic region-leucine zipper; CNC, cap'n'collar; cR, centiRays; CSKN1E, casein kinase I epsilon isoform; DEM, diethylmaleate; EH, extended homology; EMSA, electrophoretic mobility shift assays; EpRE, electrophile responsive element; EST, expressed sequence tags; LFNG, lunatic fringe; LG, linkage group; MARE, Maf recognition element; RT-PCR, reverse transcriptase-polymerase chain reaction.

* Corresponding author. Fax: +81-29-847-9195.
E-mail address: kobayash@tara.tsukuba.ac.jp (M. Kobayashi).

0006-291X/$ - see front matter © 2004 Elsevier Inc. All rights reserved.
doi:10.1016/j.bbrc.2004.05.131

[14–16], which all contain an N-terminal acidic domain that serves as a transactivation domain. Rest of the members, MafF, MafG, and MafK, constitute the small Maf protein family that possesses a bZIP motif mediating the DNA binding and dimer formation in common, but lack any recognizable transcriptional effector domains [10,17]. Both large and small Maf proteins commonly recognize a specific palindromic sequence TGCTGA(C/G)TCAGCA, called MARE (Maf recognition element) [18]. Even though the small Maf proteins do not have a transactivation domain, they affect transcription either by forming heterodimers with CNC proteins [9,18–22] or homodimers that can displace active MARE binding factors [18].

MafF, MafG, and MafK were originally identified in chicken, while mammalian homologs of these were later identified in both mouse and human, suggesting that these three paralogs are conserved among vertebrates [21,23–28]. Remarkable similarities in amino acid sequences among the three small Maf proteins have led us to speculation regarding their functional redundancy. Indeed, in vitro analyses revealed that MafF, MafG, and MafK are functionally interchangeable [10,18] and transgenic overexpression of MafK proteins could compensate for the loss of MafG in gene knockout line of mice [29].

On the other hand, null mutant mice of either *mafK* or *mafF* [26,27,30] showed no apparent phenotype, while *mafG* mutant mice displayed both mild neurological and hematological phenotypes [26]. Each small Maf gene is expressed in overlapping but distinct tissue distribution pattern during development [17,26,27], which may be the reason why disruption of the single gene *mafG* showed specific phenotypes. The *mafG::mafK* compound mutants displayed far more severe phenotypes than did mutants with the *mafG* mutation alone, implying a functional redundancy of small Maf proteins and an importance of their gene dosage [31,32]. In support of the Maf dosage hypothesis, transgenic overexpression of MafK in mice severely affected T cell proliferation and function [33], and elevation not only reduction of the small Maf protein abundance caused severe defects in megakaryopoiesis [29].

Recently, we identified both Nrf2 and Keap1 in zebrafish, demonstrating that the Nrf2–Keap1 system also regulates the expression of cytoprotective genes in fish [34]. Although there has been no report for fish small Maf proteins, four members of the large Mafs have been isolated in zebrafish [16,35,36] in addition to another member of zebrafish CNC protein p45 NF-E2 [37]. These information strongly imply that small Maf proteins may also be present in fish. Therefore, it has been of interest to know whether fish has all three small Maf proteins or not. In this study, we tried to isolate small Maf proteins in zebrafish and compare their structures with those of higher vertebrates. We identified cDNAs for four small Maf proteins in zebrafish, one MafK, and two MafG homologs in addition to a novel subtype MafT, which appears to exist specifically in fish. Interestingly, we could not find a MafF homolog in zebrafish, suggesting that both MafK and MafG are conserved among vertebrates, but not MafF is conserved in fish.

Materials and methods

Isolation of cDNAs. cDNA clones encoding zebrafish small Maf proteins were prepared by reverse transcriptase-polymerase chain reaction (RT-PCR) using total RNA from zebrafish day 4 larvae and specific primers. The primers have the following sequences: *mafk*, GGGTCG ACGACAGATTTTTGAAGAGTTCTG and 5′-GGTCTAGAGAGC ATCTCAGATTCAGATTC; *mafg1*, 5′-GGGTCGACGATTCAGAC TGTCATCTTGTG and 5′-GGTCTAGAGATGAACGACCCTGTG CTTG; *mafg2*, 5′-GGGTCGACGTTTTGCAGATCTGCGTGGC and 5′-GGTCTAGACTGCAGCTCTATGGTGCAC; and *maft*, 5′-G GGGATCCATGACTTCAGACGGCAGAG and 5′-GGGTCGACA AGCCTTCCAGCTCACGC. Several independent clones for each small Maf gene were isolated and analyzed to eliminate PCR errors. For *maft*, a cDNA library of 15–19-h stage zebrafish [38] was screened using a partial cDNA fragment as a probe to isolate full-length clone. Expression of small Maf genes was analyzed by RT-PCR as described previously [34] using following primers: *mafk*, 5′-GGGGATCCGCCAT GACGACTCATTTTAAAGC and 5′-GGTCTAGACTACGATTG TGCTGAAAAGG; *mafg1*, 5′-GGGGATCCAGGTGGAGAAGCTC GCCTC and 5′-GGCTCGAGCATTATGACCGTGCTTCTG; *mafg2*, 5′-CATGACGACCACTAATAAAGG and 5′-CTACTAAGACCTG GCGTCG; *maft*, 5′-GGGGATCCATGACTTCAGACGGCAGAG and 5′-GGGTCGACAAGCCTTCCAGCTCACGC; and *ef1α*, 5′-GCC CCTGCCAATGTA and 5′-GGGCTTGCCAGGGAC.

Fish and inducer treatment. Zebrafish embryos were obtained by natural mating. For induction studies, fish were placed in culture dishes or in tanks containing 100 μM diethylmaleate (DEM).

Plasmid construction. The plasmids pCS2mafG1, pCS2HAmafG2, pCS2mafK, pCS2mafT, and pCS2nfe2 were constructed by subcloning cDNAs for the open reading frame regions of zebrafish *mafg1*, *mafg2*, *mafk*, *maft*, and *nfe2* [37], respectively, into pCS2+ vector. In the case of pCS2HAmafG2, cDNA corresponding to HA-tag (YPYDVPDYA) was inserted after initiation ATG sequence. Other plasmids used in this study (pCS2nrf2 and pRBGP2) were described previously [18,34].

Luciferase assay. Luciferase assay was performed as described previously [34] with a slight modification. Briefly, 50 pg of the circular reporter constructs was injected alone or with synthetic capped RNAs for overexpressing transcriptional factors into embryos at the one-cell stage. Embryos were harvested at midgastrula and the luciferase activity in five embryos for each condition was determined. All luciferase activities were analyzed using the Dual-Luciferase Reporter Assay System (Promega) according to the manufacturer's instruction. Injection efficiencies were routinely normalized to the activity of a *Renilla* luciferase expression plasmid, pRL-TK. At least three independent experiments, each carried out in duplicate, were performed.

Electrophoretic mobility shift assays. Proteins were prepared by in vitro transcription and translation reactions using TNT wheat germ extract (Promega). A single MARE containing oligonucleotide (5′-TCGAGCTCGGAATTGCTGACTCATCATTACTC, identical to #25 nucleotide in Kataoka et al. [10]) was prepared by annealing synthetic oligonucleotides and ^{32}P-labeled using Rediprime II DNA Labelling System (Amersham Biosciences). Proteins were incubated with 2 fmol of ^{32}P-labeled probe at room temperature for 30 min in 20 μl of electrophoretic mobility shift assay (EMSA) binding buffer [20 mM Hepes–HCl (pH 7.6), 60 mM KCl, 4% Ficoll (4×10^5), 1 μg poly(dI–dC), and 0.66 mM dithiothreitol]. Complexes were resolved by electrophoresis on a 4% polyacrylamide gel.

Radiation hybrid mapping. Radiation hybrid mapping using panel LN54 was performed as described in Hukriede et al. [39] using specific primers for each small Maf gene. Sequences of each primer are following: *mafk*, 5′-TTGACCAAGGAAGACGTGG and 5′-CTGTGATTGGC AGACTTGAC; *mafg1*, 5′- GAGAGCTGAATCAGCACTTG and 5′-CAGCAACTTTGCCTGGTATG; *mafg2*, 5′-CCGAGTCAAGCGCG TAACG and 5′-AGACCTGGCGTCGGTCTTG; *maft*, 5′-AGGTAC AGAAGCTGAAGCAG and 5′-CTTGACTATGGTGATGACGG; and *csknle*, 5′- CTCTAGCAGAACAGCTGAGG and 5′- CTCACC AGACTGAGGTACAC.

Results and discussion

Isolation of four zebrafish small Maf cDNAs

We found four candidate genes for zebrafish homologs of small Maf proteins in the zebrafish genomic DNA (http://www.ensembl.org/Danio_rerio/) and expressed sequence tag (EST) databases (http://www.ncbi.nlm.nih.gov/dbEST/index.html). Based on the sequence information, full-length cDNA clones, *mafk*, *mafg1*, *mafg2*, and *maft* (see below for assignment and naming), were isolated by RT-PCR using total RNA from Day 4 larvae or by cDNA library screening. The percentage identity of deduced amino acid sequences between zebrafish and mouse MafK [23] was 82%, and those between zebrafish MafG1 or MafG2 and mouse MafG [26] were 88% and 85%, respectively. These results indicate that both MafK and MafG are highly conserved in the fish. The high similarity between MafG1 and MafG2 (88% identity) also suggests that the *mafg* locus was duplicated in the course of fish evolution. Fig. 1A shows multiple alignments of vertebrate small Maf proteins. From this comparison, four highly conserved regions emerge among vertebrate small Maf proteins. The extended homology (EH) and basic regions that are essential for binding to the MARE sequences [10,13,40] are conserved among the large Maf proteins. On the contrary, the other two conserved amino acid stretches, N-terminal KALKVK and C-terminal SVITIVK, were characteristic for small Maf proteins, although their functions remain to be characterized.

Sequence comparison reveals the presence of new small Maf protein MafT

An important observation was that deduced amino acid sequences of the fourth clone showed relatively low homology to all mouse small Mafs (MafK 58%, MafG 54%, and MafF 57%), suggesting that this small Maf clone may belong to a novel subfamily of small Maf proteins. While we could find a gene encoding highly homologous protein to this new small Maf in the fugu genomic DNA database (83% identity, clone number M000373 in http://fugu.hgmp.mrc.ac.uk/Analysis/), we could not find such gene in mouse, human or other vertebrate databases, implying that this subfamily is specific for teleost. We therefore named this new member of small Maf protein as MafT (small Maf in Teleost). In reverse, we could find any homologous genes to MafF neither in zebrafish nor in fugu databases (data not shown). Thus, mammals and birds have only MafF, while fish has only MafT. These results allow us to speculate that these two small Maf subfamilies might be derived from the common MafF/MafT ancestor. While genetic distance of MafF and MafT was considerably far in the phylogenetic tree (Fig. 1B), it is also possible that these two subfamilies emerged independently.

Genetic mapping of zebrafish small Maf genes

We mapped zebrafish genes for four small Mafs on the linkage map by using LN54 hybrid panel [39]. Table 1 shows the results of gene mapping. Both *mafk* and *mafg1* were mapped to linkage group 3 (LG3), 388.04 and 503.01 centiRays (cR) from the most terminal markers in each linkage group, respectively. These loci are very close to the map positions of *lfng* and *axin2*, zebrafish homologs of human lunatic fringe (*LFNG*) and *AXIN2*. Since human *MAFK* and *MAFG* are localized in close proximity of *LFNG* and *AXIN2* loci as is the case for zebrafish genes, these results argue for the presence of strong synteny between zebrafish and human genes. *mafg2* was mapped to LG11, where synteny seems not to exist with human *MAFG* or other small Maf genes. The result suggests that *mafg2* is a second MafG homolog that emerges from the fish-specific evolution. *maft* is mapped on LG12 192.54 cR from the terminal, where no adjacent gene has been mapped. Importantly, we found a 194 kb length contig of fugu genomic DNA containing puffer fish homolog of MafT gene (M000373) and a homolog for epsilon isoform of human casein kinase I (CSKN1E) gene. Human *CSKN1E* localizes on 22q13.1 where *MAFF* is also localized. We isolated a partial cDNA for the zebrafish CSKN1E homolog (*csknle*) based on information of the EST database (DDBJ/EMBL/GenBank Accession No. CF998445) and mapped its position. As expected, *csknle* was mapped to the identical position with *maft* under current resolution. These results thus support our contention that MafT and MafF are derived from a common MafF/MafT ancestor, albeit their sequences are diverged significantly during the molecular evolution.

Expression profiles of small Maf mRNAs in zebrafish

It has been shown that mouse *mafF*, *mafG*, and *mafK* exhibited distinct temporal expression profiles in developing embryos [26,27]. They also show different tissue-specific expression patterns in adult mice [27,31]. In addition, the expression of small Mafs in human and

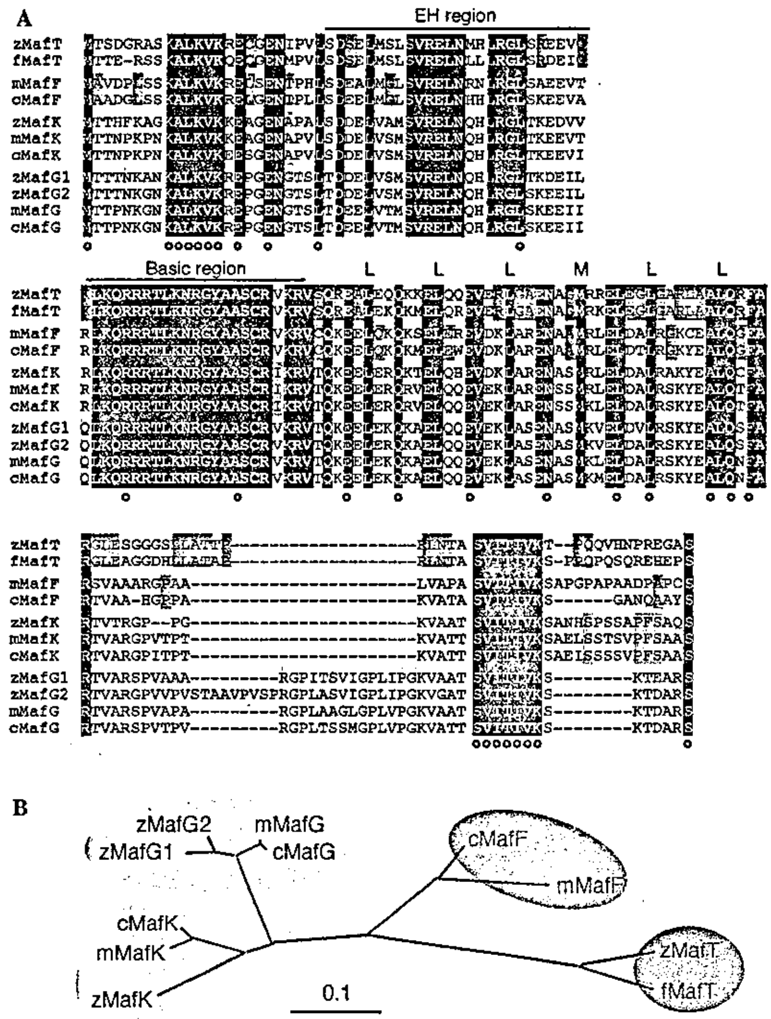

Fig. 1. Comparison of the vertebrate small Maf proteins. (A) Sequence alignment of various small Maf proteins. Conserved amino acids among all small Maf proteins are exhibited by white characters with black background, and those among only MafT, MafF, MafK, and MafG subfamilies are highlighted in purple, pink, blue and green, respectively. Amino acids highlighted in yellow indicate those conserved among MafT and MafF proteins. Open circles denote amino acids conserved among small Maf but not large Maf proteins. Heptad repeats of L or M indicate the leucine zippers. Nucleotide sequence data of *mafg1*, *mafg2*, *mafk*, and *maft* have been deposited in the DDBJ/EMBL/GenBank databases with accession numbers AB167540, AB167541, AB167542, and AB167543, respectively. (B) Phylogenetic tree of small Maf proteins. c, chicken; f, fugu; m, mouse; and z, zebrafish. Scale bar, genetic distance.

Table 1
Genetic mapping and conserved syntenies of small Maf genes

Zebrafish genes	Map positions	Human genes	Map positions
mafk	LG3-388.04 cR	*MAFK*	7p22
lfng	LG3-379.07 cR	*LFNG*	7p22
mafg1	LG3-503.01 cR	*MAFG*	17q25
axin2	LG3-501.1 cR	*AXIN2*	17q23-q24
mafg2	LG11-473.32 cR		
maft	LG12-192.54 cR	*MAFF*	22q13.1
csnk1e	LG12-192.54 cR	*CSNK1E*	22q13.1

Map positions for zebrafish *lfng* and *axin2* were cited from ZFIN Genetic Maps (http://zfin.org/cgi-bin/mapper_select.cgi), and those for human genes from NCBI human genome resources (http://www.ncbi.nlm.nih.gov/mapview/).

chicken was also demonstrated to be tissue-specific [17,21,24,25,28]. The difference in small Maf gene expression profiles led us to speculate the presence of significant variations in the regulatory mechanisms between the known small Maf genes and that of MafT. Thus, it is of interest to analyze the expression profiles of small Maf genes in zebrafish.

We therefore investigated tissue distribution of the small Maf mRNAs in adult fish. Total RNA fractions were prepared from various tissues in 7-month-old zebrafish and analyzed by RT-PCR (Fig. 2A). Amount of cDNA was standardized with the expression level of *ef1α*, a gene encoding a widely expressed translational elongation factor. While *maft* was expressed ubiquitously, its expression was relatively abundant in the

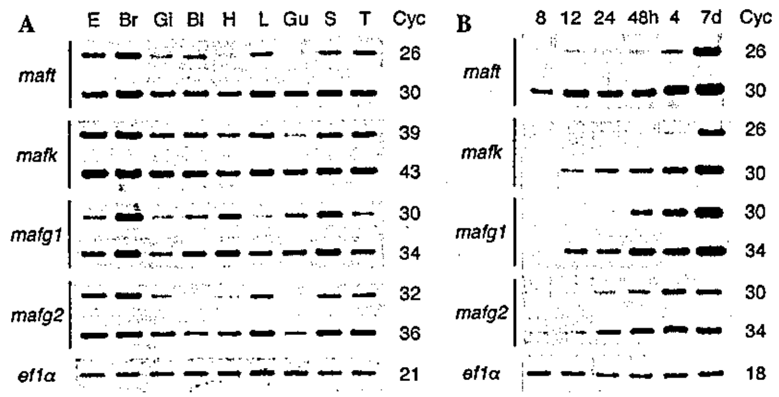

Fig. 2. Expression of small Maf mRNAs in zebrafish. Total RNA isolated from 7-month-old adult tissues (A) or whole body of embryos or larvae at the indicated developmental stages (B) was analyzed by RT-PCR using specific primers for each small Maf gene. Expression of *ef1α* was used to standardize amount of cDNA. The numbers indicate reaction cycles (Cyc) performed in the PCR. E, eye; Br, brain; Gi, gill; Bl, bladder; H, heart; L, liver; Gu, gut; S, spleen; and T, testis.

brain but scarce in the gill, heart, and gut. Expression profiles of *mafk* and *mafg2* were similar to *maft*, except a weak expression in the bladder in the case of *mafg2*. *mafg1* was also expressed ubiquitously, but of relatively high level in the heart and gut, and low level in the liver and testis in comparison with other small Maf genes.

We also examined the expression of zebrafish small Maf genes at embryonic and larval stages. RT-PCR analyses demonstrated that all Maf genes were expressed in every tested stage, but only at low level before hatching (48–72 h) during early embryogenesis (Fig. 2B).

Inducible expression of small Maf genes by DEM

In human cells or mouse tissues, the expression of small Maf genes is induced by the treatment of cells with phase 2 inducers or electrophiles [41,42]. To examine whether these inducers can also activate the expression of zebrafish small Maf genes, we analyzed expression of the small Maf genes in adult gill and whole body of larvae after treatment with DEM, a potent inducer of

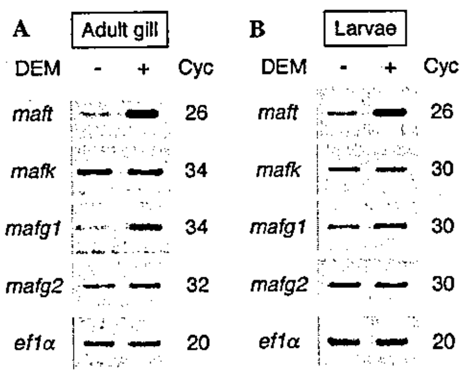

Fig. 3. Induction of small Maf genes after DEM treatment. Total RNA from adult gill (A) or whole body of larvae (B) was prepared after treatment with 100 μM DEM for 6 h and analyzed by RT-PCR using specific primers for small Maf genes.

phase 2 enzyme genes not only in mammals but also in zebrafish [34]. Fig. 3 shows that the expression of *maft* and *mafg1* was induced by the DEM treatment. This result indicates that regulatory mechanisms of small Maf genes are conserved among vertebrate. It is also consistent with the previous report, in that the induction level of each small Maf gene was varied among human cell lines [42]. While we could not find a significant difference in responsiveness to DEM between adult and larvae, *maft* in zebrafish showed highest induction level among small Maf genes. This observation shows very good agreement with that of *MAFF* in human cells [42].

Activity of MafT protein to heterodimerize with CNC proteins and bind to DNA

We then carried out to assess the ability of MafT and other zebrafish small Maf proteins forming homodimers or heterodimers with the known members of the zebrafish CNC proteins, i.e., Nrf2 and p45 Nfe2 [34,37], exploiting a single MARE containing oligonucleotide [10] as a probe (Fig. 4). Formation of homodimers was observed in the case of MafT and MafK, but it was not obvious for MafG1 nor MafG2 (Fig. 4, lanes 4, 7, 10, and 13, arrow). The weakened activity of MafG1 and MafG2 to form homodimers may be due to insolubility of homotypic full-length proteins under the conditions used for EMSA, since this was also observed when we examined mouse or chicken MafG proteins (data not shown) [10]. When we tested heterodimer formation of zebrafish small Maf proteins with CNC proteins, appearance of slower migrating bands was found upon the addition of Nrf2 to the reaction mixture (Fig. 4, closed arrowheads). These bands correspond to Nrf2-small Maf heterodimers, since specific antibodies for Nrf2 and small Mafs abolished the bands (data not shown). Similarly, an additional band to the homodimer band was observed after combining p45 Nfe2 to the reaction